

# CLOUD CAPACITY SPECTRUM METHOD: ACCOUNTING FOR RECORD-TO-RECORD VARIABILITY IN FRAGILITY ANALYSIS USING NONLINEAR STATIC PROCEDURES

Andrea Nettis<sup>1\*</sup>, Roberto Gentile<sup>2</sup>, Domenico Raffaele<sup>1</sup>,  
Giuseppina Uva<sup>1</sup>, Carmine Galasso<sup>2,3</sup>

<sup>1</sup>Department of Civil, Environmental, Land, Building Engineering and Chemistry,  
Polytechnic University of Bari, Italy

<sup>2</sup>Department of Civil, Environmental and Geomatic Engineering & Institute for Risk and Disaster Reduction.  
University College London, London, United Kingdom

<sup>3</sup>Scuola Universitaria Superiore (IUSS) Pavia, Italy

This paper investigates some computational issues related to the use of nonlinear static procedures in fragility analysis of structures. Such approaches can be used to complement nonlinear dynamic procedures, reducing the computational and modelling effort. Specifically, this study assesses the performance of the Capacity Spectrum Method (CSM) with real (i.e., recorded) ground motions (as opposed to code-based conventional spectra) to explicitly account for record-to-record variability in fragility analysis. The study focuses on single-degree-of-freedom systems, providing a basis for future multi-degree-of-freedom system applications. A case-study database of 2160 inelastic oscillators is defined through parametric backbones with different elastic periods, (yield) base shear coefficients, values of the ductility capacity, hardening ratios, residual strength values and hysteresis rules. These case studies are analysed using 100 real ground motions. An efficient algorithm to perform the CSM with real spectra is proposed, combined with a cloud-based approach (Cloud-CSM) to derive fragility relationships. Simple criteria to solve the issue of multiple CSM solutions (i.e., two or more points on the backbone satisfying the CSM procedure) are proposed and tested. It is demonstrated that the performance point selection can be performed based on a particularly efficient intensity measure detected via optimal intensity measure analysis. The effectiveness of the proposed Cloud-CSM in fragility analysis is discussed through extensive comparisons with nonlinear time-history analyses, the code-based N2 method, and a simple method involving an intensity measure as a direct proxy for the performance displacement. The Cloud-CSM provides errors lower than  $\pm 20\%$  in predicting the median of the fragility curves in most of the analysed cases and outperforms the other considered methodologies in calculating the dispersion.

## KEYWORDS

Fragility analysis, nonlinear static procedures, probabilistic seismic assessment, capacity spectrum method, parametric analysis, time-history analysis

## 1. INTRODUCTION AND MOTIVATIONS

In seismic vulnerability modelling and risk assessment applications, fragility relationships for a considered structure or structural type express the probability of reaching or exceeding a damage state (DS) given a value of the earthquake-induced ground-shaking intensity. Numerical approaches to derive fragility relationships are currently widespread and typically preferred to empirical approaches given the scarcity of high-quality post-earthquake damage data for various earthquake-prone regions of the world. Such numerical approaches generally rely on a probabilistic seismic demand model calibrated on a dataset of engineering demand parameter (EDP) vs ground-motion intensity measure (IM) pairs. Various EDPs of interest can be computed through refined nonlinear dynamic or simplified nonlinear static analysis methods. Nonlinear dynamic approaches enable the prediction of structure- or structural component-specific EDPs for an appropriately selected/modified suite of ground-motion records through nonlinear time history analyses (NLTHA) of a computational structural model. Conversely, nonlinear static procedures (NSPs) investigate the structural capacity of an equivalent single-degree-of-freedom (SDoF) system of the investigated structure under incremental load patterns, enabling the prediction of the seismic performance (in terms of EDPs) through demand spectrum-based approaches. The former approach is arguably the most advanced/accurate one but generally requires high modelling efforts (i.e., to define the nonlinear model of the structure under investigation), apart from being computationally more expensive than NSPs. The latter approach is simpler/practical, but it generally results in biased

\*Correspondence to: Andrea Nettis, Polytechnic University of Bari, andrea.nettis@poliba.it

EDP estimates due to the various assumptions in the method, such as the selection of an appropriate load pattern representative of the effects of a dynamic excitation or the definition of an equivalent SDoF system [1].

60 In the case of large-scale applications (e.g., assessing the seismic performance and the risk of large building portfolios in a region), an analyst has to make a trade-off between computational costs and the (desired) accuracy of the assessment, for instance regarding the considered number of sample structures to properly represent a structural type (or building class) and the considered seismic analysis technique [2]. For example, depending on the resource availability (in terms of computational and modelling time and skills), an analyst may consider 1) a large population of structures analysed through NSPs, trying to capture the building-to-building variability (e.g., [3]); or 2) few archetype (or index) structures analysed through nonlinear dynamic procedures. It is envisaged that nonlinear dynamic  
65 procedures will be the preferred option and become prevalent in practice in the near future due to increasing available high-performance computing and required expertise. Alternatively, a hybrid approach could allow using different model classes (e.g., few dynamic analyses and many static ones) combined in a Bayesian framework to derive robust fragility estimations (e.g., [4]).

70 NSPs generally are based on approximate approaches for the inelastic performance displacement prediction of SDoF systems and can be divided into two categories. The first category includes methods that estimate the maximum displacement demand under a given seismic action by multiplying the displacement demand of an equivalent secant-to-nominal-yielding period linear system by some modification factors. For instance, the well-known N2 method [5,6] employs an elastic-perfectly plastic SDoF idealisation of actual pushover curves (i.e. relationships between global base shear and displacement of a control node), which is subsequently used to estimate the inelastic equivalent SDoF  
75 performance displacement. In its original version, this latter is estimated via NLTHA of the equivalent SDoF. However, a code-based simplified approach (Eurocode 8 part 3 [7]) adopts ductility-based modification factors and demand-spectra for predicting the equivalent SDoF performance displacement. Similarly, the Displacement Coefficient Method (DCM), proposed by the Federal Emergency Management Agency (FEMA-273 [8]), adopts a bilinear idealisation of equivalent SDoF pushover curves and uses modification factors accounting for the bias  
80 involved by the SDoF idealisation, influence of inelasticity, cyclic degradation of strength and stiffness, P-delta effects. The second category includes methods that calculate the target displacement of inelastic systems as the over-damped response of elastic SDoF systems having secant-to-target displacement stiffness. The Capacity Spectrum Method (CSM) [9] has been implemented in different guidelines (e.g., ATC-40 [10] and FEMA-440 [11]); it is conceptually based on overdamped spectra calculated through equivalent viscous damping coefficients expressing the reduction of seismic demands caused by the inelastic response of the structure under investigation. Starting from a bilinear idealisation of pushover curves, the CSM involves an iterative procedure to identify a performance point (PP)  
85 indicating the equivalent SDoF performance displacement of the structure. The CSM has also been slightly modified [12] to be implemented together with adaptive pushover procedures. For both the categories, several studies carried out in the last decades proposed formulations that can improve the estimation of equivalent SDoF target displacement  
90 (e.g. [13–16]). Further research efforts focused on comparing the accuracy and practicality of these different methodologies (e.g. [17,18]) within a displacement-based design or assessment framework, but not for fragility estimations.

As pointed out in recent discussions by experts in vulnerability analysis (e.g., [2]), NSPs usually do not account for record-to-record variability since smooth code-based design spectra conventionally represent the seismic demand.  
95 Consequently, within a fragility analysis framework, only a central value of the fragility relationship can be estimated (e.g., the IM corresponding to a 50% probability of violating a DS of interest if a lognormal model is used). In this case, conventional values of variance, calibrated for different structural types, are usually introduced for describing the lognormal probabilistic model [2]. To fill this gap, hybrid methodologies based on pushover analysis of MDoF systems together with NLTHA performed on sets of equivalent SDoF systems (to consider aleatory and epistemic  
100 uncertainties) have been recently proposed [19,20]. In this context, Vamvatsikos and Cornell [21] proposed a semi-empirical analytical approach for predicting the median and record-to-record variability of peak response of SDoF systems represented by multi-linear backbones. A set of equations based on specific backbone parameters is provided for approximating incremental dynamic analysis curves corresponding to 16, 50 and 84% fractiles.

To the authors' knowledge, only a few studies in the literature investigated the effectiveness and shortcomings of  
105 using NSPs with real (i.e., unsmoothed, record-specific) response spectra to estimate nonlinear seismic performance and to represent record-to-record variability in fragility analysis explicitly. In the Global Earthquake Model (GEM) guidelines [22], an approach to derive a probabilistic seismic demand model through the N2 method is described with application to low/mid-rise buildings. Silva et al. [1] investigated the effectiveness of different NSPs applied with real response spectra in deriving fragility relationships and risk/loss estimations considering record-to-record variability  
110 for a class of typical Turkish reinforced concrete-framed buildings. A stripe-based approach is used in [23] for fragility analysis through the CSM with reference to existing reinforced concrete frames. Recently, Giordano et al. [24] applied

the CSM for fragility analysis of masonry buildings in Nepal, adopting real spectra modified by smoothing-spectrum procedures.

In the context of probabilistic seismic risk assessment, and with the overall aim of explicitly accounting for record-to-record variability in fragility analysis through NSPs, this study investigates the CSM use with ground motion-specific spectra to estimate the nonlinear seismic performance of various case-study structural systems. Specifically, this study focuses on simple inelastic SDoF systems representative of various structural types. A database of 2160 case-study systems defined through parametric multi-linear backbone curves and different hysteresis rules is considered together with 100 ground motions selected from the Selected Input Motions for displacement Based Assessment and Design (SIMBAD) database [25] to represent strong ground-motion records of engineering relevance.

It is worth mentioning that different error sources can be detected when deriving CSM-based fragility estimates for MDoF structures. Among others, these are a) the transformation of the refined MDoF pushover curve to the SDoF multi-linear one; b) the simplified SDoF performance displacement prediction for any given SDoF pushover curve, including the cases of multiple CSM solutions if as-recorded spectra are used [26]; c) the fitting of a probabilistic seismic demand model and fragility curve(s). This study only involves a bias quantification for b), as well as b) coupled with c). The analysis of the error source a) is considered out of scope here, although crucially needed and worthy of investigation. For practical applications on MDoF structures, deemed to be the scope of CSM-based fragility analysis, error source a) should be carefully checked on a case-by-case basis before extensive parametric studies are available. A first evaluation of the error source a) with reference to four- and eight-story reinforced concrete frames is reported in [27].

Findings from the present study can directly support fragility analysis applications where the SDoF idealisation based on the analysed structures' elastic or effective modal properties is a convenient practice. This is, for example, the case of recently proposed displacement-based approaches (e.g., [28–30]) aimed at the seismic design/assessment of different structural typologies or applications which adopt an SDoF-based modelling strategy (e.g. [31,32]) to consider building-to-building variability in fragility models of structural typological classes. The adopted investigation scheme to address the CSM use for fragility analysis is reported in Figure 1. Each block corresponds to a specific section of the study. First, the SDoF case-study database is described. In Section 3, an algorithm to effectively adapt the CSM for use with real spectra is proposed, and different criteria to select the PP in multiple-solution cases are described, based on simple assumptions or efficient IM parameters identified via an optimal IM analysis. Moreover, a description of the adopted cloud approach, proposed by Jalayer et al. [33], to compute probabilistic seismic demand models via the CSM (Cloud Capacity Spectrum Method, or Cloud-CSM) is presented. The last part of the paper includes an extensive discussion of results to guide interested users in applying the proposed method in practice. Specifically, Section 4 investigates the effectiveness of the criteria to perform the PP selection and discusses both the case of individual ground-motion records and the fragility analysis. In Section 5, the accuracy of the Cloud-CSM in performing fragility analysis is investigated. To this aim, the main parameters of the fragility curves calculated employing the Cloud-CSM are compared to the results achieved using the N2 method applied with real spectra, a simple approach involving an IM as a direct proxy for the performance displacement, and NLTHA. Finally, Section 6 provides recommendations for practical applications of the proposed Cloud-CSM.

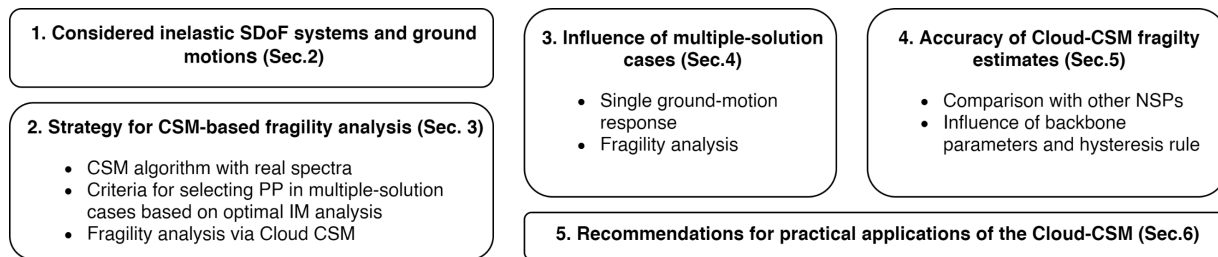


**Figure 1. Investigation scheme and contents of the study (CSM: capacity spectrum method, NSP: Nonlinear static procedures).**

150

## 2. CONSIDERED INELASTIC SDOF SYSTEMS AND GROUND MOTIONS

The case-study database developed for this study includes simple inelastic SDoF systems with different nonlinear behaviour, represented by a multi-linear backbone curve and a hysteresis rule. Various hysteresis rules are used to simulate the seismic response of different structural types (Figure 2) [30]. Two different types of Modified Takeda

155

hysteretic behaviour [34] are selected. The “thin” version (Figure 2a, herein indicated as MTt) is appropriate for structures with high axial stress (such as bridge piers, structural walls, or masonry structures), while the “fat” one (Figure 2a, MTf) is used in the case of ductile RC frames [30]. Two backbone types of kinematic hardening hysteretic behaviour are selected: a bilinear (BIL) and an elastic-perfectly-plastic (EPP) hysteresis laws (Figure 2b). These are used to represent the cyclic flexural response of steel structures (neglecting the Bauschinger effect in the members) or seismic isolated structures (with elastomeric bearings or friction pendulum systems). A flag-shaped (FS) law is finally selected (Figure 2c) for simulating the cyclic behaviour of hybrid prestressed structures. The parameters defining the backbones (Figure 2) are the elastic period  $T_{el}$  (related to the elastic stiffness  $K_{el}$ ), the base shear coefficient  $F_y$  (yield base shear strength normalised by the total weight), the ductility capacity  $\mu$ , the hardening ratio  $r$  and the normalised residual strength  $F_r$ . The assumed values for each parameter are listed in Table 1. Since no strength degradation may be considered for low-damage structures, the softening and residual strength branches are not accounted for within the FS subgroup, and the backbone curve is modified accordingly (Figure 2c). In this case, the ductility parameter is only used to define the DS thresholds. Note that in the case of BIL, EPP and FS no cyclic stiffness degradation is adopted. In summary, 720 (i.e., eight periods  $\times$  five base shear coefficients  $\times$  three values of ductility  $\times$  three hardening values  $\times$  two values of residual strength) oscillators are associated with the MTt and MTf; 240 cases are considered for the BIL subgroup (where only a hardening equal to 10% is fixed) and for the EPP (zero hardening by definition); a total of 240 oscillators corresponds to the FS subgroup (Table 1).

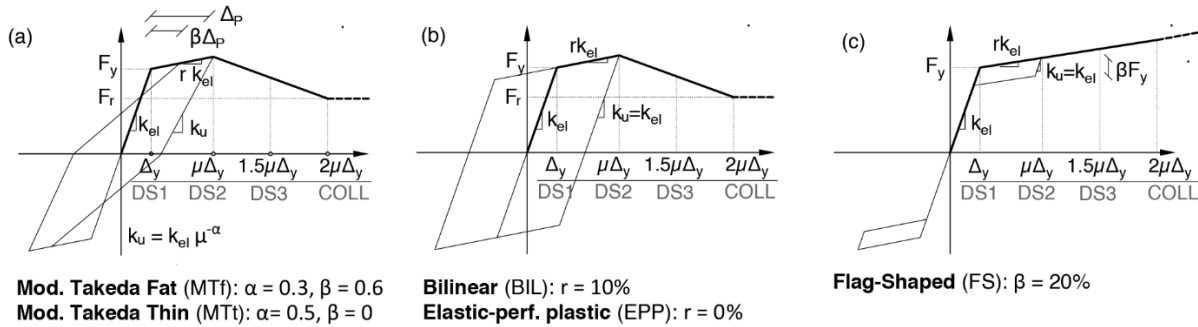


**Figure 2. Parametric backbone curves and cyclic behaviour of the considered case-study subgroups: a) modified Takeda (fat and thin), b) bilinear and elastic-perfectly plastic, c) flag-shaped**

In this study, a suite of 100 unscaled ground motions is used, selected from the SIMBAD database. This includes 467 tri-axial records related to 130 worldwide seismic events (shallow crustal earthquakes) with moment magnitudes ranging from 5 to 7.3 and epicentral distance minor than 35 km. In this study, 100 records are selected by first ranking the 467 records in terms of their PGA values (by using the geometric mean of the two horizontal components) and then (arbitrarily) keeping the component with the largest PGA value (for the 100 stations with highest mean PGA). Figure 3 shows the spectra of the selected ground motions. The spectral accelerations corresponding to the case-study  $T_{el}$  and the yield accelerations ( $a_y = F_y * g$ ) adopted in the case-study dataset are also represented to provide an insight into the nonlinear demand on the case studies. Note that the probabilistic seismic demand models (reported in the following sections) of cases with high values of elastic period and base shear coefficient can be biased given the low number of ground motions leading to an inelastic response. Although this could be solved by scaling the intensity of the adopted records, this is not done herein to avoid considering unrealistically strong records. This record selection strategy is compatible with the adopted cloud-based approach, which does not require a hazard-specific record selection and therefore, it is widely accepted for portfolio analyses. Although such an approach can create a bias in the analysis results, this may be mitigated after running the response analysis [35]. The peak ground accelerations of the selected ground-motion suite range between 0.29 g and 1.77 g. A total of 216000 NLTHA (100 accelerograms  $\times$  2160 oscillators) are performed using the nonlinear finite element software RUAUMOKO3D [36] using nonlinear spring models equipped with appropriate multi-linear backbones and cyclic behaviour. As suggested by Priestley et al. [30], a constant 5% tangent stiffness proportional damping is selected for all the frequencies.

**Table 1. Parameters defining the backbone curves and assumed values**

	MTt	MTt	BIL	EPP	FS
$T_{el}$	0.25, 0.5, 0.75, 1, 1.25, 1.5, 1.75, 2 s				
$F_y$	0.1, 0.2, 0.3, 0.4, 0.5				

$\mu$	1.5, 3, 4.5			
$F_r$	0.6 $F_y$ , 0.3 $F_y$			No softening
$r$	0%, 5%, 10%	10%	0%	0%, 10%

195

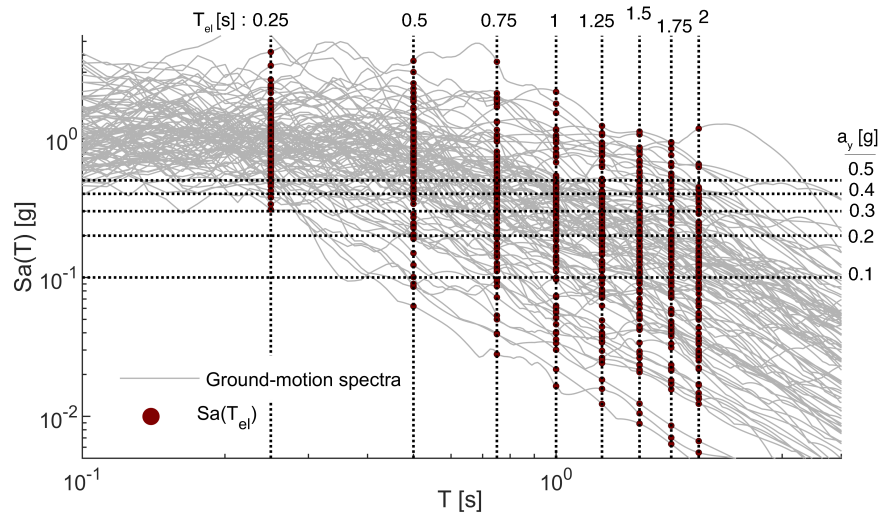


Figure 3. Ground-motion spectra, spectral accelerations at the case-study elastic periods  $T_{el}$  and case-study yielding accelerations ( $a_y$ ).

### 3. CSM FOR FRAGILITY ANALYSIS

200 In this section, the CSM algorithm suitable to predict record-specific performance with real spectra is presented. Different criteria to select the PP in multiple-solution cases are defined. These are based on both simplistic assumptions or a particularly efficient IM, identified via an optimal IM analysis described in Appendix A. Finally, an overview of the cloud-based methodology (Cloud-CSM) to perform fragility analysis is presented.

#### 205 3.1 Proposed Algorithm for the CSM

The CSM aims to determine the performance of a structure under a given seismic input represented by a response spectrum. ATC-40 [10] originally proposed three different procedures (A, B and C) to apply the CSM. A brief description of procedure A, which is considered the most convenient to be implemented in simple spreadsheets, is outlined in this section. It requires the computation of a pushover curve (i.e., force vs displacement) for the investigated structure, which can be obtained through a pushover analysis. The pushover curve is converted into the so-called “capacity spectrum” of an equivalent SDoF system expressed in an acceleration vs displacement format. The CSM consists of an iterative graphical procedure aimed at determining the PP in an acceleration-displacement plane through overdamped spectra. First, a tentative performance displacement is assumed. A bilinearisation of the capacity spectrum up to the tentative performance displacement is carried out to obtain the equivalent yielding displacement. The ductility demand corresponding to the tentative performance displacement is calculated. Then, an overdamped demand is computed by multiplying the elastic demand (generally a code-based smooth spectrum) for a spectral reduction factor ( $\eta$ ), derived from a ductility-based equivalent viscous damping coefficient ( $\xi$ ) which expresses the reduction of the elastic demand given the hysteretic dissipation. A new performance displacement is calculated as the intersection between the overdamped demand and capacity spectra. If the calculated performance displacement is sufficiently close to the guessed one (within a tolerance arbitrarily assumed by the analyst), the algorithm stops. Otherwise, the calculated performance displacement is used as the new tentative target displacement, and another iteration is carried out. The process continues until the convergence is achieved. The final PP expresses the compatibility between the overdamped demand and ductility-based equivalent viscous damping of the structure.

225 In this study, the CSM is slightly modified to be applied with real demand spectra. Note that multiple solutions could be obtained when using real spectra, as mentioned in [11,12,26,37]. Obviously, multiple solutions are not physics-based since the PP represents the structure’s response under a given ground-motion input. Thus, to apply the CSM with real spectra, a final additional step might be needed, if multiple solutions are obtained, to select the PP. Since

230 such an iterative process could be unstable in the case of multiple solutions [26], an alternative algorithm is herein proposed to easily identify the solution(s) (Figure 4a). Note that other noniterative approaches for performing the CSM were proposed (e.g. [14]). These are based on a direct closed-form estimation of the secant-to-target period, depending on the strength ratio between an equivalent elastic response and the actual one. However, these formulations are developed for EPP hysteretic response only and, to the authors' best knowledge, have not been tested for other hysteresis rules.

235 A preliminary step of the procedure requires identifying the yielding point using an equivalent bilinear or multi-linear relationship of the capacity spectrum of the structure [38]. Clearly, if the spectrum intersects the elastic branch of the capacity spectrum, an elastic response of the SDoF system is registered, and the PP can be straightforwardly identified. If no elastic solutions are detected, the capacity spectrum is discretized in small displacement intervals ( $\Delta_{i+1} = \Delta_i + d\Delta$ ) from the yielding point to the ultimate capacity corresponding to different damping levels. The amplitude of  $d\Delta$  is arbitrarily selected by the analyst and corresponds to the accuracy of the final result (i.e., the final performance displacement can be expressed as  $\Delta_{PP} \pm d\Delta$ ). In this study,  $d\Delta = 0.001$  m is adopted. An equivalent elastic SDoF oscillator can be associated with each  $\Delta_i$ , characterised by an effective period ( $T_{eff,i}$ ), an equivalent viscous damping ( $\xi_i$ ) and a spectral reduction factor ( $\eta_i$ ).  $T_{eff,i}$  is calculated via Equation 1 where  $\mu_i$  is the ductility demand at  $\Delta_i$ . There is an extended research literature on the approaches for the calculation of  $\xi$  and  $\eta$ , adapted for various specific structural typologies [39–41]. In this study, the approach proposed in [30] is used, which is based on a simple ductility-based formulation calibrated for different hysteretic behaviour. The  $\xi_i$  and  $\eta_i$  are thus calculated through Equation 2 and 3 respectively, where the adopted  $C_{evd}$  values are reported in Table 2.

$$T_{eff,i} = \sqrt{\frac{\mu_i}{1 + r(\mu_i - 1)}} T_{el} \quad (1)$$

$$\xi_i = 0.05 + C_{evd} \left( \frac{\mu_i - 1}{\pi \mu_i} \right) \quad (2)$$

$$\eta_i = \sqrt{\frac{0.07}{0.02 + \xi_i}} \quad (3)$$

250 For each equivalent SDoF system, the acceleration-displacement components of the elastic demand are interpolated at the effective period  $T_{eff,i}$  and are multiplied by  $\eta_i$ , generating the overdamped demand at  $T_{eff,i}$ . Thus, a “variable-damping spectra” is obtained collecting the acceleration-displacement pairs of the overdamped demand calculated for each value of  $T_{eff,i}$ . The CSM solution(s) are the intersections between the capacity spectrum and the variable-damping spectra. If no intersections are found, the structure is unable to sustain the applied ground-motion input. Figure 4b presents three sample ground motions selected for illustrative purposes: one solution (elastic and inelastic, respectively) is associated with records #3 and #6, while record #10 produces multiple solutions. The issue of choosing the PP is addressed in Section 3.2, examining different criteria.

**Table 2. Values of  $C_{evd}$  for the adopted hysteresis rules [30]**

	MTt	MTt	FS	EPP	BIL
$C_{evd}$	0.444	0.565	0.186	0.670	0.519

260

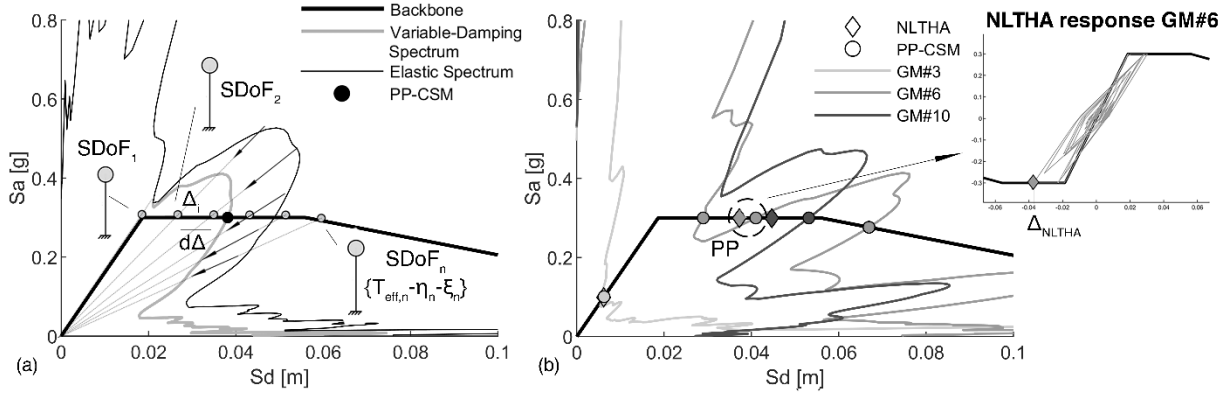


Figure 4. a) Graphical representation of the proposed algorithm to perform the CSM, b) examples of single and multiple CSM solutions.

### 3.2 Candidate criteria to select the PP

265 Six candidate criteria to select the PP dealing with multiple-solution cases are herein defined and assessed. These criteria should be simple enough to enable a fast, possibly automatized, selection of the PP within a fragility analysis framework involving a large number of ground motions. The criteria are proposed based on a particularly efficient IM and simplistic assumption. The adopted IM is based on the geometric average of spectral displacements over an appropriate range of periods ( $AvgSd_k$ ), calculated using Equation 4. Consistently with [42], ten equally spaced periods (270  $N = 10$ ) are used to compute  $AvgSd_k$ . The efficiency of  $AvgSd_k$  is evaluated through the optimal IM analysis reported in Appendix A.

$$AvgSd_k = \left( \prod_{i=1}^N Sd(T_i) \right)^{\frac{1}{N}} \text{ with } T_i \in \left[ T_{el}, \sqrt{Sd(T_{el})/\Delta_y T_{el}} \right] \quad (4)$$

275 • The first criterion (C1) is the most refined one. Regression analysis is carried out to provide a simple relation between the NLTHA-based ductility demand,  $\mu_{TH}$  and two predictors linked to both the demand (ground motion spectrum) and significant backbone parameters of the single SDoF. Initially, the pairs of ground motion-SDoF system characterised by inelastic demand are selected. Nonlinear regression is performed according to the parametric model proposed in Equation 5 via the least square method. The ratio between  $AvgSd_k$  and the yielding displacement of the specific SDoF,  $\Delta_y$ , and the elastic period  $T_{el}$  are assumed as 280 the predictors for  $\mu_{TH}$ . The values of the parameters  $[a, b, c, d]$ , calculated for the different hysteresis subgroups, together with the corresponding coefficient of determination  $R^2$  are presented in Table 3. The PP is the CSM solution whose ductility demand best mimics the results of the proposed regression model.

$$\mu_{TH} = (a T_{el} + b) * \left( \frac{AvgSd_k}{\Delta_y} \right)^{c T_{el} + d} \quad (5)$$

285 • The second criterion (C2) assumes that, for specific ground motion, the PP is the one for which  $|AvgSd_k - \Delta_{PP}|$  is minimum.

• The first and the last solutions on the backbones are assumed as the PP within the third (C3) and fourth (C4) criteria, respectively. These criteria are proposed to evaluate if it is worth performing a more accurate selection consistently with C1 and C2.

290 • The last criterion (C5) foresees that the record-specific performance can be approximated by the arithmetic average of the displacements provided by the various solutions.

Table 3. Parameters of the regression-based formulation and  $R^2$  for C1 (Equation 5).

	MTt	MTt	FS	EPP	BIL
$a$	-0.030	-0.028	-0.021	-0.036	-0.055

<i>b</i>	1.059	1.033	1.098	1.082	1.095
<i>c</i>	0.023	0.034	0.017	0.017	0.056
<i>d</i>	0.860	0.831	0.876	0.751	0.685
$R^2$	0.8156	0.8275	0.8643	0.7487	0.8008

### 295 3.3 Cloud-based procedure for fragility analysis

For each specific SDoF system, a cloud of EDP vs IM points is retrieved. The adopted IM is the geometric average of the spectral accelerations  $AvgSa$ , whose efficiency, sufficiency and hazard computability were extensively discussed in recent literature studies for fragility analysis of various structural types. Given the results of the optimal IM analysis (Appendix A),  $AvgSa$  is computed in the interval  $[T_{el} - 1.5T_{el}]$  and it can be calculated via Equation A2, by replacing  $Sd(T_i)$  with  $Sa(T_i)$ . The EDP is the performance displacement calculated employing NLTHA or the target displacement corresponding to the PP calculated via the CSM. Three DS thresholds (also indicated in Figure 2, Section 2) are defined, corresponding to the yielding point ( $\mu_{DS1} = 1$ ), the peak strength point ( $\mu_{DS2} = \mu$ ) and half of the softening branch ( $\mu_{DS3} = 1.5\mu$ ). The cloud-based procedure proposed by Jalayer et al. [33] is adopted in this study to perform fragility analysis. The cloud data are divided into “collapse” and “no-collapse” to derive the fragility functions. Collapse herein corresponds to a global dynamic instability of the numerical analysis detected by NLTHA (mainly due to  $P - \Delta$  effects for SDoFs) or exceeding a conventional displacement threshold. This is equal to the reaching of the residual strength branch ( $\mu_{collapse} = 2\mu$ ). Equation 6 shows the generic analytical form used in this study for a given fragility relationship, where the probability of violating a given DS,  $P(EDP \geq edp_{DS}|IM)$ , is calculated applying the total probability theorem, aggregating the probability of reaching or exceeding the DS for the non-collapse cases,  $P(EDP \geq edp_{DS}|IM, NoC)$ , and the probability that the collapse occurs,  $P(C|IM)$  [33]. Note that since all the collapse cases certainly exceed the DS threshold ( $edp_{DS}$ ),  $P(EDP \geq edp_{DS}|IM, C)$  is equal to 1. The fragility model related to the non-collapse cases is expressed by the normal cumulative distribution function  $\phi(\cdot)$  based on the probabilistic seismic demand model for non-collapse cases. This latter is calculated by fitting a power-law model,  $EDP = aIM^b$ , for the non-collapse cases in the  $\log IM - \log EDP$  plane [33]. The parameters  $a$  and  $b$  are estimated through regression analysis resorting to the least square method. The dispersion  $\sigma_{NoC}$  is calculated through Equation 7 using the  $edp_{gm} - im_{gm}$  pairs corresponding to the  $gm$ -th record.  $P(C|IM)$  is computed by fitting a logistic regression model suitable to binary (collapse-no collapse) variables.

$$\begin{aligned}
P(EDP \geq edp_{DS}|IM) &= P(EDP \geq edp_{DS}|IM, NoC)(1 - P(C|IM)) + P(EDP \geq edp_{DS}|IM, C)P(C|IM) = \\
&= \phi\left(\frac{\ln edp_{DS} - \ln a im^b}{\sigma_{NoC}}\right)(1 - P(C|IM)) + P(C|IM)
\end{aligned} \tag{6}$$

$$\sigma_{NoC} = \sqrt{\frac{\sum_{gm=1}^N (\ln edp_{gm} - \ln a im_{gm}^b)^2}{N - 2}} \tag{7}$$

320 Consistently with the study by Jalayer et al. [33], the probabilistic seismic demand model representing the median EDP (having the 50% probability of being reached,  $edp^{50}$ ) given IM, considering both collapse and non-collapse cases, can be calculated with Equation 8.

$$edp^{50} = a im^b \cdot \exp(\sigma_{NoC} \cdot [0.5/(1 - P(C|IM))]) \tag{8}$$

325 To facilitate the analysis of the results,  $P(EDP \geq edp_{DS}|IM)$  is in turn approximated with a lognormal cumulative distribution function, whose median ( $\alpha$ ) and dispersion ( $\beta$ ) can be used to compare the large number of fragility curves calculated for all the case studies. To this aim,  $\alpha$  represents the value of IM corresponding to a 50% exceedance probability of a given  $edp_{DS}$  and it is calculated via Equation 6 by setting the left side equal to 0.5.  $\beta$  expresses the “slope” of the fragility relationship and is approximated as half of the difference between the logarithmic values of IM corresponding to the 84% and 16% exceedance probability (left side of Equation 6 equal to 0.84 and 0.16).



#### 4. DISCUSSION ON THE CSM ANALYSES WITH MULTIPLE SOLUTIONS

335 The issue of the multiple solutions detected with the CSM is addressed in this section. First, the effectiveness of the  
previously described criteria (Section 3.2) to identify the PP is discussed. In the second sub-section, the sensitivity of  
the fragility curves to the percentage of multiple-solution cases within the ground motion suite is studied.

##### 4.1 Effectiveness of the proposed criteria in single ground-motion response

340

The large analysis database is filtered to consider only the cases (combinations of SDoF oscillators and ground-motion  
records) for which multiple CSM solutions are detected. The PP is selected according to the various criteria (from C1  
to C5). The accuracy of the single criterion is assessed by comparing the chosen PP with the benchmark criterion (C0),  
that is considered the theoretically best solution (benchmark PP). C0 implies the manual selection of the PP, which  
best mimics the NLTHA result. Note that the cases in which the benchmark PP is a collapse case are excluded.

345

Moreover, the cases characterised by multiple solutions which are all detected beyond the collapse threshold are  
excluded and directly considered as collapse cases (rather than multiple solution cases). First, a preliminary discussion  
about the influence of significant backbone parameters and expected equivalent viscous damping on the occurrence  
of multiple solutions is reported. Figure 5 relates the percentage of multiple-solution cases (calculated as the number  
of ground motions producing multiple solutions divided by the total number of adopted records), varying elastic  
period, ductility and the base shear coefficient for MTf and FS subgroups (representative of high- and low-dissipation).

350

Figure 5 is related to the oscillators having  $F_r$  and  $r$  equal to  $0.6F_y$  and 0% respectively (selected for illustrative  
purposes). It is worth mentioning that the outcomes reported in Figure 5 could be strictly linked to the amplitude and  
frequency content of the specific ground motions used in this study. It is evident that the number of multiple solutions  
decreases as the elastic period increases. This is influenced by the higher number of elastic responses detected for  
longer-period structures. The cases having an elastic period higher than 1.00 s are not considered in the figure since  
they exhibit a negligible number of multiple solutions (less than 5%). For the MTf, it is shown that the 0.25 s-period  
cases exhibit the highest percentage of multiple solutions. This percentage rises as the base shear coefficient and  
ductility capacity increase, with a maximum of 37% for  $F_y$  equal to 0.5 and  $\mu$  equal to 4.5. An opposite trend is  
detected for 0.75 s-period cases where the percentage of multiple solutions reaches a maximum of 12% for  $F_y$  and  $\mu_c$

355

equal to 0.3 and 1.5, respectively. For the FS, the number of multiple-solution cases strongly decreases, with a  
maximum of 15% for the case with  $T_{el}$  equal to 0.25 s and  $F_y$  equal to 0.5. In this case, the number of intersections  
between the variable-damping spectra and the backbone decreases. This may be caused by the low cyclic dissipation  
capacity and the absence of the softening branch. It is worth mentioning that the results for other hysteresis subgroups  
are similar to the results shown for MTf (the differences in the percentage of multiple-solution cases are less than 5%).  
Moreover, the reported results are only slightly sensitive to the hardening and residual strength values with variations  
less than 5% within each period-strength-ductility subgroup.

360

To discuss the effectiveness of the proposed criteria in selecting the PP for a single ground-motion response, the results  
are grouped by elastic period and hysteretic behaviour. The effectiveness of each criterion is evaluated through the  
mean of the ratios ( $\hat{R}$ ) between  $\Delta_j^{C0}$  and  $\Delta_j^{Ci}$  which are the performance displacements related to the benchmark C0  
and the generic criterion respectively, for the  $j$ -th case (ground motion-oscillator pair showing multiple solutions). It  
is calculated via Equation 9 where  $N_{ms}$  is the number of multiple-solution cases for a determined subgroup of  
oscillators. The best performing criterion is the one with  $\hat{R}$  closest to one.

365

370

Figure 6 extensively reports the indexes  $\hat{R}$  for all the period-hysteresis subgroups. Different markers correspond to the  
considered criteria, while the variation of colours indicates different hysteresis rules. The effectiveness of C1 is shown  
by the corresponding  $\hat{R}$  included in the range [0.94;1.08], demonstrating the accuracy of the regression models  
described in Section 3.2. The effectiveness of C2 is particularly evident for low/medium-period ( $T_{el} \leq 1.25$  s)  
oscillators ( $0.99 \leq \hat{R} \leq 1.04$ ), while a loss of accuracy is registered for high-period cases ( $T_{el} \geq 1.50$  s) characterised  
by EPP and BIL hysteresis behaviour ( $\hat{R} \geq 1.08$ ). Although its simplicity, C3, which implies the selection of the  
lowest performance displacement, provides a satisfactory accuracy with respect to C0. Indeed, in this case, an  
overestimation of the performance displacement in the range [2%; 14%] ( $0.86 \leq \hat{R} \leq 0.98$ ) is observed, with the  
maximum error registered for EPP at  $T_{el}$  equal to 0.50 s. In contrast, if the last PP (largest displacement) is chosen

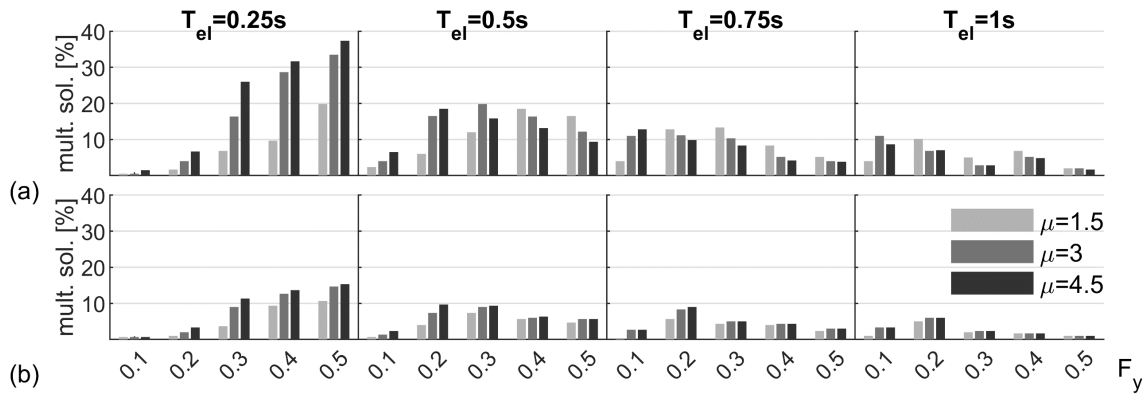
375

$$\hat{R}_{Ci} = \frac{1}{N_{ms}} \sum_{j=1}^{N_{ms}} \Delta_j^{Ci} / \Delta_j^{C0} \quad (9)$$

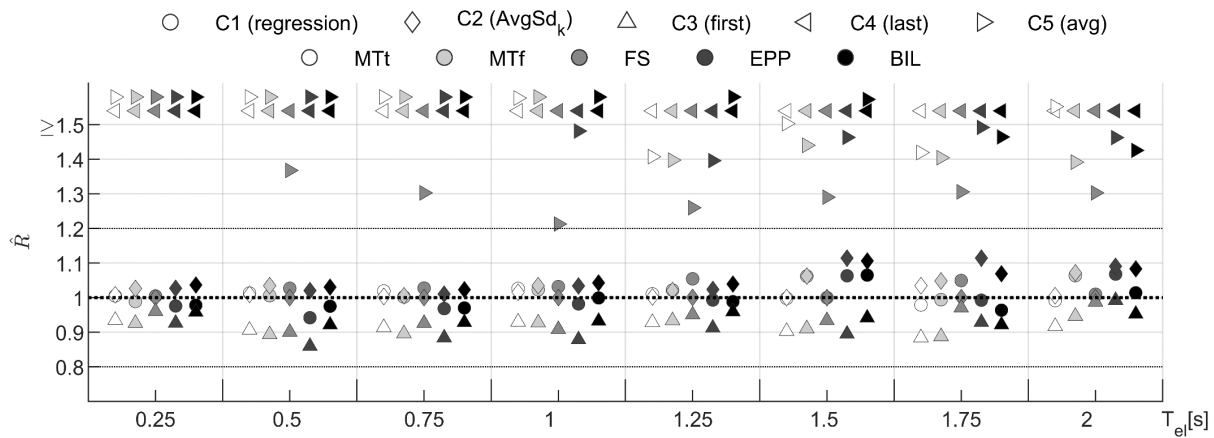
380

Figure 6 extensively reports the indexes  $\hat{R}$  for all the period-hysteresis subgroups. Different markers correspond to the  
considered criteria, while the variation of colours indicates different hysteresis rules. The effectiveness of C1 is shown  
by the corresponding  $\hat{R}$  included in the range [0.94;1.08], demonstrating the accuracy of the regression models  
described in Section 3.2. The effectiveness of C2 is particularly evident for low/medium-period ( $T_{el} \leq 1.25$  s)  
oscillators ( $0.99 \leq \hat{R} \leq 1.04$ ), while a loss of accuracy is registered for high-period cases ( $T_{el} \geq 1.50$  s) characterised  
by EPP and BIL hysteresis behaviour ( $\hat{R} \geq 1.08$ ). Although its simplicity, C3, which implies the selection of the  
lowest performance displacement, provides a satisfactory accuracy with respect to C0. Indeed, in this case, an  
overestimation of the performance displacement in the range [2%; 14%] ( $0.86 \leq \hat{R} \leq 0.98$ ) is observed, with the  
maximum error registered for EPP at  $T_{el}$  equal to 0.50 s. In contrast, if the last PP (largest displacement) is chosen

385 (i.e., C4), a noticeable loss of accuracy is registered and a displacement overestimation higher than 50% ( $\hat{R} \geq 1.50$ ) is generally expected regardless of the elastic period and hysteresis rule. Finally, C5 leads to values of  $\hat{R}$  included in the range [1.2;1.4] for the FS subgroup and higher for other hysteresis rules. Indeed, C5 provides  $\hat{R}$  higher than 1.5 for low-period cases ( $T_{el} \leq 0.75$  s) for MTt, MTf, EPP and BIL hysteresis rules.



390 **Figure 5. Percentage of multiple-solution cases on varying period, ductility capacity and base shear coefficient for MTt (a) and FS (b) subgroups ( $F_r = 0.6F_y$ ;  $r = 0\%$ ).**



**Figure 6.  $R$  indexes of the candidate criteria for all the hysteresis-period subgroups.**

#### 4.2 Influence of multiple solutions on fragility analysis

395 Since the outcomes of the previous sub-section are limited to a single ground-motion response analysis, further tests are needed to definitively demonstrate the accuracy of the different criteria in fragility analysis which is the target of this study. The influence of the number of multiple solutions and of the adopted PP selection criterion in fragility analysis is discussed herein. The fragility curves for DS1, DS2 and DS3 are calculated for all the considered SDoF systems according to the procedure outlined in Section 3.3, selecting the PP according to the previously described criteria. If the selected PP exceeds the collapse threshold, it is classified as collapse. The criterion C0 is taken as a benchmark. It is worth mentioning that the oscillators characterised by at least one ground motion leading to multiple solutions are selected to perform this task (approximately 75% of the cases; only extremely high-period high-strength cases are excluded). Figure 7 helps in understanding the expected effect of the multiple-solution cases in the fragility analysis. This shows the cloud data ( $\Delta_{pp} - AvgSa$ ; collapse cases are indicated with squared markers beyond the collapse threshold) and the probabilistic seismic demand models (calculated via Equation 8) of two sample cases having an elastic period equal to 0.25 s and 0.75 s with 44% and 14% of multiple solutions, respectively. Only the results for the criteria C2, C3, C4 and C0 are reported. In both cases, it is evident that the  $\Delta_{pp}$  chosen according to C2 and C3 generally overlap with C0, so that the estimated power-law models are similar, with increasing differences approaching DS3. In Figure 7a, several of the  $\Delta_{pp}$  associated with C4 differ with respect to the other criteria producing

400

405

410

different estimations of the parameters of the power-law models. Since in this case C4 overestimates the displacement demand, it provides lower values of the median IM at all the three DSs. As expected, this effect is less evident in the case shown in Figure 7b, where the percentage of multiple solutions is lower than the previous one.

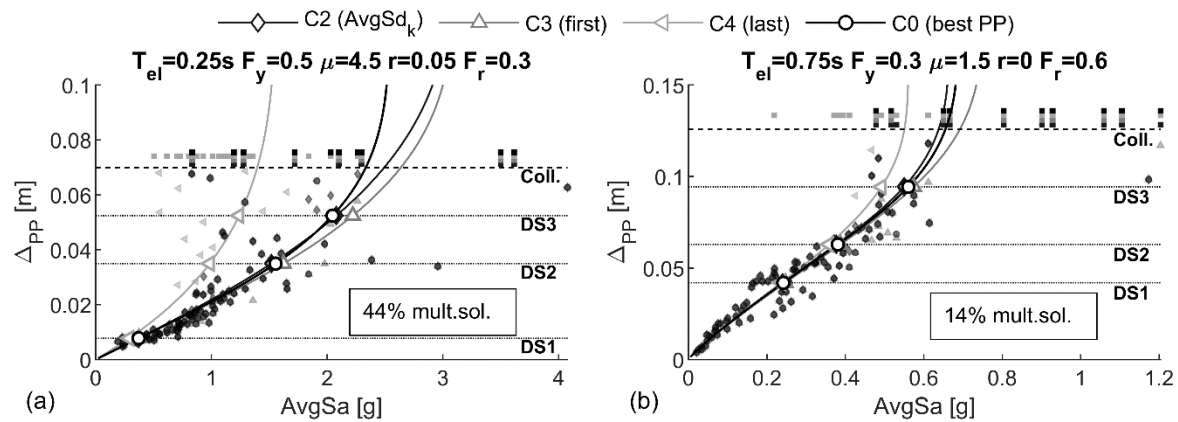


Figure 7. CSM-based probabilistic seismic demand models of two sample SDoF systems within the MTF subgroup.

415

To systematically investigate the accuracy of the different selection criteria, the relative error between the median IM ( $\alpha$ ) and the dispersion ( $\beta$ ) estimated by means of the  $i$ -th criterion ( $C_i$ ) and C0 is calculated. The results are discussed in terms of relative error vs percentage of multiple solutions within the 100 ground motions adopted. As indicated in Figure 8, the error data, indicated with markers having different shades of grey, are grouped in intervals having 10% amplitude, and piecewise trend lines are calculated (through the least square method). Figure 8 shows the error trends on the median IM value for the MTF subgroup with reference to DS1 (Figure 8a) and DS3 (Figure 8b). For DS1, C1, C2 and C3 provide errors lower than 5% regardless of the percentage of the multiple solutions. In contrast, the deficiencies of C4 and C5 strongly increase with the number of multiple solutions leading to average errors higher than 30%, tending to a percentage of multiple solutions equal to 40%. For DS3, the most accurate criteria are C2, and C1, with errors lower than +5 and +8%, respectively. C5 is the worst criterion providing errors which increase from -18% to -35% for 30% to 40% percentage of multiple solutions. Finally, C3, although its simplicity, provides errors lower than +10% with a negligible increase for increasing percentages of multiple-solution cases.

420

425

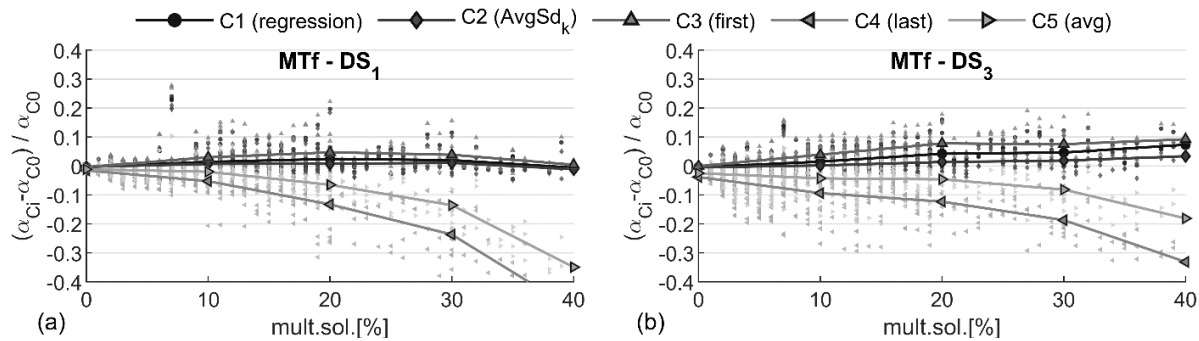


Figure 8. Relative errors on the median of the fragility curves related to the percentage of multiple-solution cases at DS1 (a) and DS3 (b) for the MTF subgroup.

430

Figure 9 reports the trend lines for the relative errors on  $\alpha$  related to the MTt, BIL, EPP and FS subgroups. The grey trend lines refer to DS1, while the red lines to DS3. It is shown that the results for MTt, BIL and EPP are particularly similar to MTF as, for instance, demonstrated by the poor performance of C4 and C5 for an increasing number of multiple solutions. For FS, the low number of multiple solutions implies that the average expected error is lower than 15%, independently of the selection criterion. Finally, Figure 10 reports the relative errors in terms of dispersion  $\beta$  for DS3 with reference to MTF (Figure 10a) and BIL (Figure 10b). It is evident that C4 considerably overestimates the dispersion from 10% to 50% approaching 40% of multiple solutions. Differently, C1, C2 and C3 provide 5% errors

435

on average. A similar trend is reported for the other subgroups having different hysteretic behaviours (not shown for brevity).

440 These outcomes extend the recommendations by Casarotti et al. [12], suggesting selecting the PP corresponding to the largest displacement (i.e., C4) in multiple-solution cases as a conservative choice. Indeed, it is shown that C4 (and also C5) may considerably overestimate the fragility of the investigated structure with a noticeable loss of accuracy depending on the percentage of multiple solutions. On the other hand, C1, C2 and C3 can consistently reduce the bias induced by the multiple solutions. Although C1 provides good accuracy, it is the most demanding in terms of calculation effort and does not involve consistent improvements with respect to C2 and C3. C3 provides good accuracy, but its results could be not conservative. To conveniently limit the bias induced by the multiple solutions, C2 is recommended, allowing a quick but accurate selection of the PP.

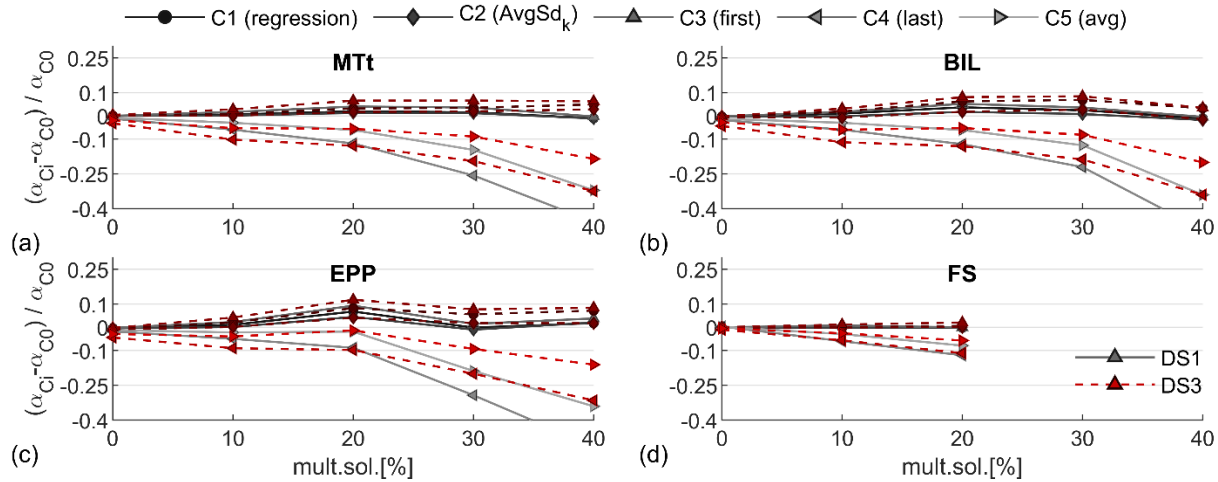


Figure 9. Relative errors on the median IM related to the percentage of multiple-solution cases at DS1 (continuous grey) and DS3 (dashed red) for the MTt (a), BIL (b), EPP (c), FS (d) subgroups.

450

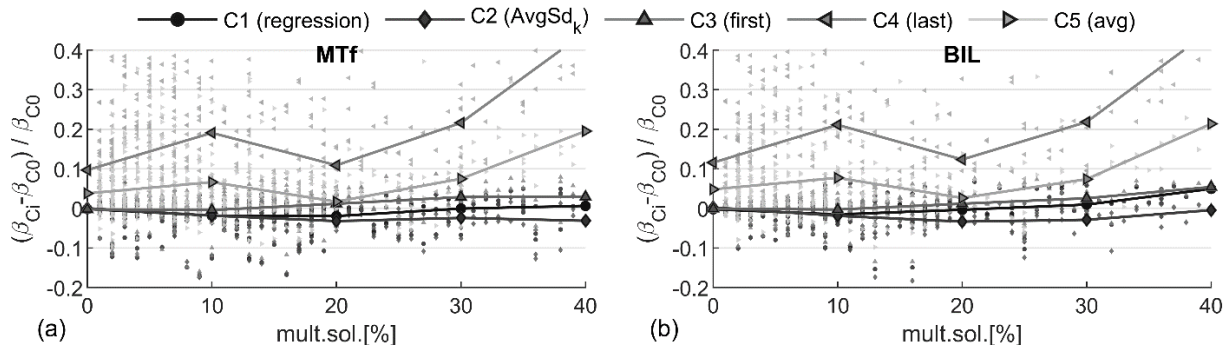


Figure 10. Relative errors on the dispersion ( $\beta$ ) of the fragility curves on varying percentage of multiple solutions at DS3 for the MTf (a) and BIL (b) subgroups.

## 5. EFFECTIVENESS OF THE CLOUD-CSM FOR FRAGILITY ANALYSIS

455 The fragility analysis is performed for each SDoF system in the dataset. This task is carried out using the performance displacements calculated through the proposed algorithm for the CSM (Section 3.1), NLTHA and two other NSPs: the N2 method and the IM-based method. If multiple solutions are derived with the CSM, the C2 criterion, which requires the selection of the nearest solution to the proposed  $AvgSd_k$  is used to select the PP. The fragility analysis is performed according to the cloud-based procedure in Section 3.3. The median ( $\alpha$ ) and the dispersion ( $\beta$ ) are used to systematically compare the differences in the fragility functions calculated with the different approaches. Given the wide database of SDoF systems, the oscillators are grouped based on significant backbone parameters and hysteresis rules to efficiently discuss the results.

460

## 5.1 N2 method with real spectra and proposed IM-based approach for performance displacement evaluation

465

In this study, the effectiveness of the CSM is discussed with reference to the widespread code-based version of the N2 method as included in Eurocode 8 part 3 [7]. This method is described in this sub-section, focusing on its application with real spectra to compute fragility functions as discussed in [22]. The N2 method is based on capacity spectra, obtained from MDoF pushover curves converted in SDoF format and, differently from the CSM, exploits displacement modification factors for predicting the inelastic SDoF displacement. This latter can be identified by a PP on the capacity spectrum, as for the CSM.

470

First, the capacity spectrum is simplified in an elastic-perfectly plastic law to determine the elastic period and yielding displacement of the investigated structure. The PP is estimated depending on the relation between the elastic period and the corner period of the adopted elastic (usually code-based) spectrum ( $T_c$ ) which is the period at the end of the constant-acceleration part. If the elastic period is higher than the corner period, the equal-displacement rule is applied, and the target displacement is equal to the spectral displacement at the elastic period  $Sd(T_{el})$ . On the other hand, if the elastic period is lower than the corner period, two conditions may occur. If the spectral acceleration is lower than the yielding capacity of the system, an elastic response is expected, and the target displacement equals the spectral displacement, again. In contrast, the formulation by Vidic et al. [43] is applied, and the target displacement is calculated with Equation 10 where  $q_u$  is the ratio between the elastic spectral acceleration and the yielding acceleration.

475

480

$$\Delta_{PP} = \frac{Sd(T_{el})}{q_u} \left( 1 + (q_u - 1) \frac{T_c}{T_{el}} \right) \geq Sd(T_{el}) \quad (10)$$

485

This methodology is usually applied with smooth code-based spectra, where the interval of periods related to the constant acceleration section (from  $T_B$  which is the lowest period of the constant acceleration part, to  $T_c$ ) of the spectrum is known. Since this interval is not defined for real spectra, the strategy proposed by Calvi et al. [44] for the calculation of  $T_c$  of real spectra is used.  $T_c$  is defined at the intersection between a line at 90% of the maximum spectral acceleration and the response spectrum in the spectral acceleration-period plane. Since more than one intersection will occur, the lowest period should be chosen. In this study, the simplified approach implemented in the code-based N2 method is applied to calculate the performance of multi-linear SDoF systems in which the elastic branch is known. Consequently, the MDoF-SDoF conversion strategy is not applied, and the bilinearisation is directly performed, neglecting the contribution of the hardening and the softening.

490

To further benchmark the CSM, another NSP-based methodology is proposed, identified herein as IM-based method. It is based on the results of the optimal IM analysis in Appendix A, which demonstrated  $AvgSd_k$  as the most efficient IM. It envisages that the performance displacement of an SDoF system under a given ground-motion input is simply equal to the value of  $AvgSd_k$  calculated through Equation 4. Similarly to the N2 method, this approach requires the knowledge of the elastic period and the multiplying factor ( $\sqrt{Sd(T_{el})/\Delta_y}$ ) for the period elongation related to the considered record. It is worth noting that both the N2 and IM-based methods require less computational efforts than the CSM. The comparison among these methodologies aims to evaluate whether it is worth performing a more accurate and computationally demanding CSM algorithm.

495

500

## 5.2 Comparison with other nonlinear static procedures and influence of the yield base shear coefficient

505

This sub-section shows the sensitivity of the accuracy of the Cloud-CSM with respect to the yield base shear coefficient, which is the most critical backbone parameter affecting the inelastic response. The results for the oscillators having a medium value of ductility ( $\mu = 3$ ), a maximum value of residual strength ( $F_r = 0.6F_y$ ), no hardening ( $r = 0\%$ ) and MTt hysteresis rule (representative of moderate hysteretic dissipation) are selected for illustrative purposes.

510

Figure 12 quantifies the relative errors on the median IM between the considered NSPs and NLTHA calculated at the reaching of the three DSs (indicated with different markers) for all the considered oscillators grouped by period. Figure 12 reports the probabilistic seismic demand models related to three sample cases, appropriately selected to better understand the results shown in Figure 12. In Figure 12, the cloud data are reported with filled markers, graphically differentiated in collapse (squared markers) and non-collapse cases (circular markers). The median values of the fragility curves are represented with empty markers at the intersections between the probabilistic seismic demand models and the dotted horizontal lines, which indicate the DS thresholds. The cases with  $T_{el}$  equal to 0.25 s and  $F_y$  lower than 0.2, together with those with  $T_{el}$  equal to 0.50 s and  $F_y$  equal to 0.1 are excluded from the database of

515

results, since more than half of the  $\Delta_{PP} - AvgSa$  pairs exceed the collapse thresholds, thus preventing a robust fitting of the probabilistic seismic demand model [33]. In the remaining 0.25 s-period cases, the CSM and IM-based method lead to errors included in the range [-20%;10%], while the N2 provides errors higher than +20% at DS3. Figure 12a, which refers to a short-period high-strength oscillator, shows that the CSM overestimates the NLTHA-based displacement demands resulting in lower values of  $\alpha$  with errors equal to -19% and -20% for DS2 and DS3, respectively. Contrarily, the N2 method underestimates the NLTHA displacement demand for the entire range of IM, thus resulting in an error on  $\alpha$  equal to +20% for DS3. The IM-based method outperforms the N2 (the maximum error with respect to NLTHA is -10% for DS2), proving that in this case  $AvgSd_k$  is a better proxy of the inelastic response with respect to the simpler  $Sd(T_{el})$ , since it accounts for the spectral shape in the range of period elongation.

In most of the cases with  $T_{el}$  between 0.50 s and 1.00 s, the CSM provides high accuracy, with errors included in the range [-10%;10%], outperforming the other methods. As an example, Figure 12b reports the cloud data and probabilistic seismic demand models for the oscillator having  $T_{el}$  equal to 0.75 s and  $F_y$  equal to 0.2. It is observed that the CSM-based probabilistic seismic demand model nearly matches with the NLTHA-based one, providing a maximum error of 4% on  $\alpha$  at DS3. The IM-based method underestimates the median of the fragility curve with a maximum error equal to -9% at DS2. In contrast, for the DS3 and collapse thresholds, the probabilistic seismic demand model estimated by the N2 strongly diverges from the other methods. This is also confirmed by the lower number of collapse cases (7) predicted by this method with respect to the CSM (11) and NLTHA (13).

Figure 12 shows that the accuracy of the N2 and IM-based methods increase with increasing base shear coefficient and the resultant decreasing inelastic response. This is also demonstrated by the results corresponding to high-period ( $T_{el} \geq 1.25$  s) cases, where the N2 outperforms both the IM-based method and the CSM. Figure 12c represents the probabilistic seismic demand models of an oscillator with a long period ( $T_{el} = 1.50$  s) and low strength ( $F_y = 0.1$ ). In this case, N2 provides the best accuracy with negligible errors with respect to the NLTHA-based probabilistic seismic demand model. The CSM significantly underestimates the displacement demands for higher values of the considered IM, overestimating the value of  $\alpha$  with errors equal to +10%, +20% and +22% at DS1, DS2 and DS3, respectively. In contrast, the IM-based method underestimates the median with a maximum -14% error at DS3. As shown by Figure 12, a significant loss of accuracy of the CSM is generally observed for all the oscillators having  $T_{el}$  higher than 1.25 s and  $F_y$  equal to 0.1. However, the accuracy of the CSM consistently increases for a higher value of yield base shear strength, producing errors lower than 20% when  $F_y$  is higher than 0.2.

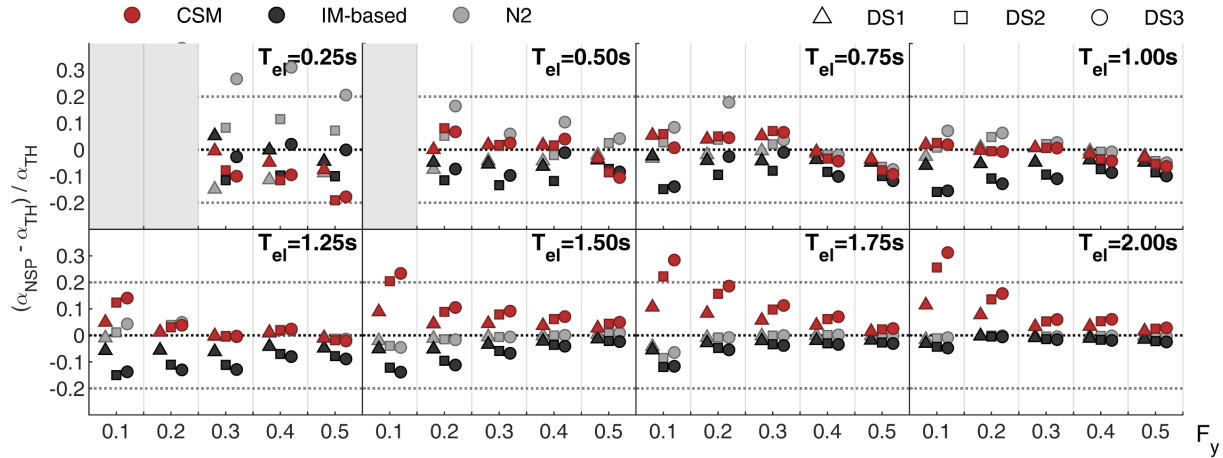


Figure 12. NSP-vs-NLTHA relative errors on the median  $IM(\alpha)$  for the SDoF systems characterised by  $\mu = 3$ ,  $F_r = 0.6F_y$ ,  $r = 0\%$  and MTt hysteresis rule.

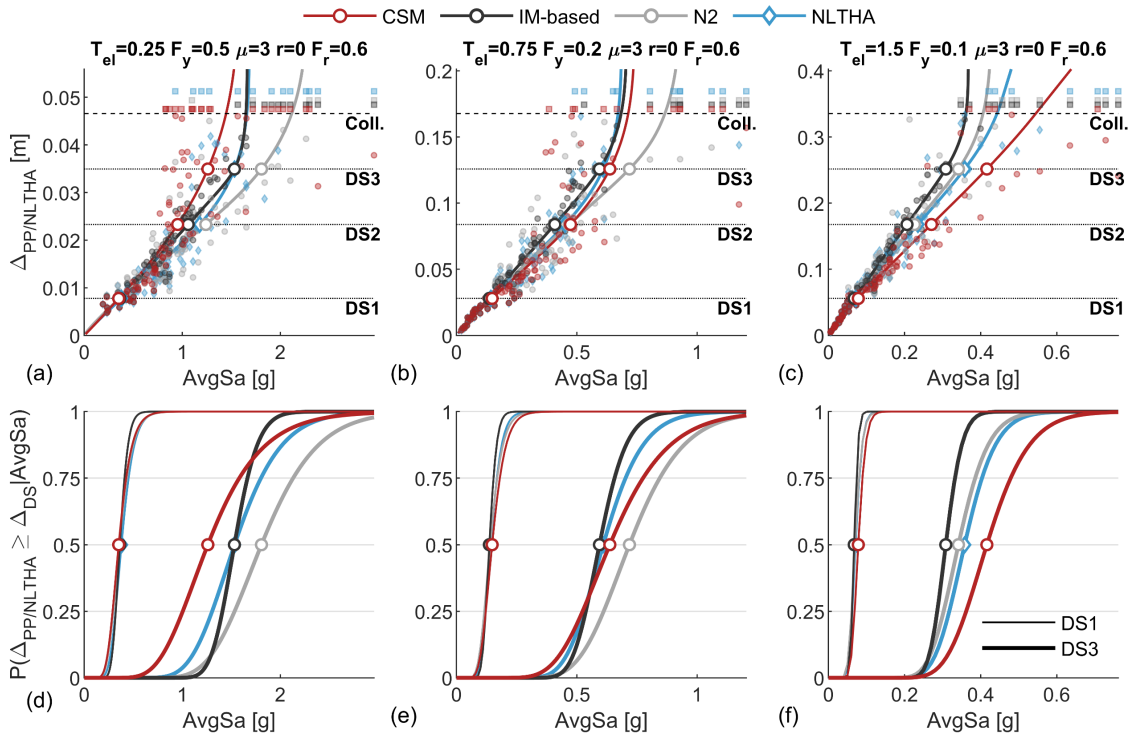


Figure 12. Probabilistic seismic demand models (a, b, c) for three selected sample SDoF systems and corresponding fragility curves (d, e, f).

545

To further evaluate the divergences in the fragility curves calculated using the NSPs and NLTHA, the differences in the dispersion  $\beta$  are shown in Figure 13. According to the procedure described in Section 3.3, the global dispersion for a given DS accounts for the contribution of the lognormal cumulative distribution function and the logistic function modelling the collapse/no collapse variable. It is proved in this study that the former term, which is conventionally assumed constant among the different damage states [22], is the most significant contribution to  $\beta$ . Consequently, slight differences are registered among the dispersions calculated at the different DSs. As an example, with reference to the cases shown in Figure 12,  $\beta_{DS1}$  and  $\beta_{DS3}$  are 0.26 - 0.24, 0.24 - 0.20 and 0.18 - 0.17 for the first (a), second (b) and third (c) case, respectively. For this reason, the following discussion is addressed to DS3 only. It is worth noting that strategies to derive fragility dispersion estimates depending on the IM level are proposed in the literature (e.g. [22,45,46]) and those can be easily included in the Cloud-CSM.

550

555

Figure 13a shows the values of  $\beta_{DS3}$  calculated assuming  $AvgSa$  as an IM. It is observed that the differences in calculating the dispersion become negligible with increasing base shear coefficient and elastic period. Particularly, in short-period cases, the CSM overestimates the NLTHA-based dispersion, and it seems that in these cases, the N2 outperforms the CSM providing negligible errors with respect to the NLTHA. The dispersion provided by the IM-based method is always lower than 0.2, underestimating the one calculated employing NLTHA. On the other hand, Figure 13b refers to a fragility analysis carried out using  $Sa(T_{el})$  as an IM. In this case, N2 provides very low dispersion with respect to the NLTHA, while a better accuracy is evident for the IM-based method. This low value of  $\beta_{DS3}$  is due to an increasing correlation between EDP and IM. Indeed, if the equal-displacement rule is applied, the performance displacement provided by the N2 is equal to  $Sd(T)$ , which is perfectly correlated to the  $Sa(T)$  used as IM ( $Sa(T) = (2\pi/T)^2 Sd(T)$ ). The value of  $\beta_{DS3}$  gradually decreases for increasing elastic periods and increasing relevance of the equal-displacement rule in calculating the cloud data. Similarly, the low dispersion of the IM-based method when the  $AvgSa$  is used as IM can be explained by an increasing correlation between EDP and IM. It can be stated that NSPs that calculate the seismic performance of the investigated structure based on simple spectral ordinates can strongly underestimate the effect of record-to-record variability in the dispersion of fragility curves, thus resulting in potential underestimation of the seismic risk. In contrast, the CSM-based performance displacement is not dependent on the adopted IM type since this method does not resort to spectral ordinates calculated at a given period(s) to calculate the performance displacement. Indeed, a general overestimation of the NLTHA-based dispersion is registered both if  $Sa(T_{el})$  or  $AvgSa$  are used as IM. Particularly, with reference to Figure 13a, the registered overestimation decreases as the base shear coefficient and elastic period increase. The errors with respect to NLTHA increase if a less efficient IM is adopted (such as  $Sa(T_{el})$ ) in cases for which a considerable period elongation is expected. Note that an increasing dispersion is on the safe side with reference to seismic risk calculation. Consequently, this error can be considered an acceptable trade-off for reducing computational effort associated with the CSM with respect to NLTHA.

580

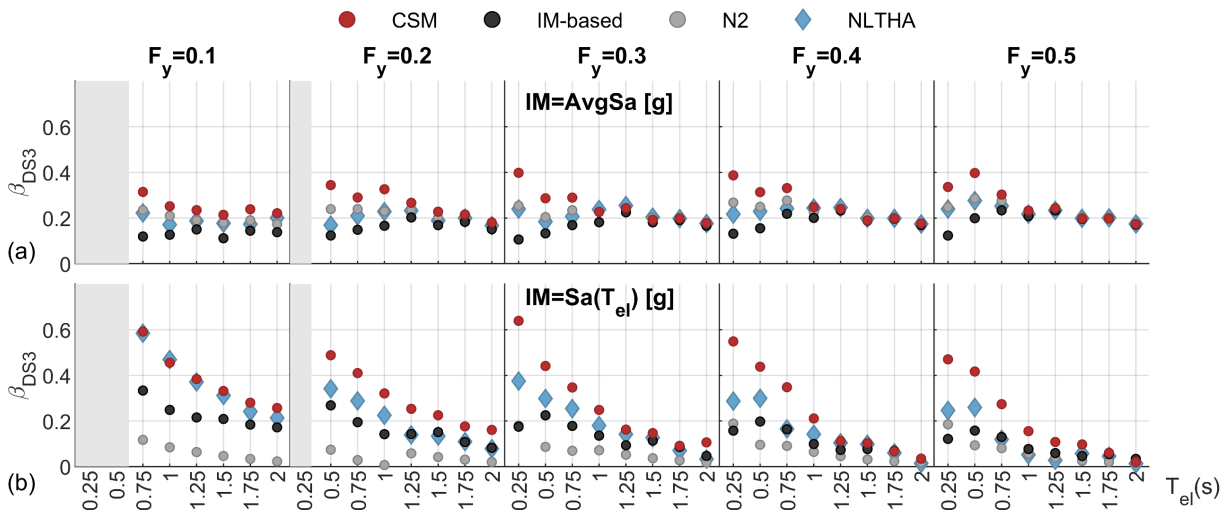


Figure 13. Dispersion ( $\beta$ ) calculated at DS3 estimated by the NSPs and NLTHA for the considered MTt subgroup ( $\mu = 3, F_r = 0.6F_y, r = 0\%$ ) using  $AvgSa$  (a) and  $Sa(T_{el})$  (b) as IM.

### 5.3 Influence of the hysteresis rule

In this sub-section, the sensitivity of the effectiveness of the Cloud-CSM to the hysteretic behaviour is discussed. This is directly reflected in an evaluation of the accuracy in predicting the NLTHA-based results of the different equivalent viscous damping coefficients associated with the considered hysteresis rules. To synthetically address this topic, the results discussed in this section refers particularly to the oscillators having the intermediate value of ductility ( $\mu = 3$ ), the maximum residual strength ( $F_r = 0.6F_y$ ) and 0% hardening (except for the BIL subgroup where a hardening equal to 10% is considered). It is worth mentioning that, differently than the CSM, the N2 and IM-based methods do not consider modifications in the seismic performance due to different hysteresis rules, thus providing the same target

590



displacement regardless of the cyclic response. In other words, the fragility curves calculated via these methods do not change among the considered hysteresis subgroups.

595 Figure 14 reports the results for the MTf and BIL subgroups (which exhibit comparable values of  $C_{evd}$ ) for the cases having an elastic period equal to 0.25 s, 0.50 s (short period), 1.00 s (medium period) and 1.50 s (high period). Both Figure 14a (MTf) and Figure 14b (BIL) show that the CSM generally provides good accuracy for the cases with a short-medium elastic period leading to errors on  $\alpha$  lower than 20%. Also, in these cases, a loss of accuracy is registered for low-strength cases with high elastic periods. As an example, for the oscillator having an elastic period equal to 1.50 s and the base shear coefficient of 0.1, the CSM provides errors for DS3 equal to 22% and 27% for MTf and BIL, respectively. Since the hysteretic dissipation associated with MTf and BIL slightly differ from MTt (see Table 2), these results generally agree with the outcomes shown in Figure 12. This also implies that the accuracy of the N2 and IM-based methods (providing the same target displacement for all the hysteresis rules) registered for the MTt subgroup is approximately confirmed for MTf and BIL.

600 Figure 15 reports the results for the FS and EPP, which are characterised by considerably different hysteretic behaviour with respect to the cases previously analysed. Referring to the FS, higher values of the CSM performance displacements are expected given the low hysteretic dissipation ( $C_{evd} = 0.186$ ). In this case, Figure 15a shows that the CSM properly estimates (with errors included in the range [-18%;12%]) the NLTHA-based median IMfor cases with an elastic period equal to or higher than 0.5 s. In contrast, the N2 systematically overestimates it, with the error increasing for strong inelasticity. This evidences the general accuracy of the equivalent viscous damping proposed by Priestley et al. [30] for an FS hysteresis rule and the low reliability of  $Sd(T_{el})$  in estimating the seismic performance of low-dissipation structures. Note that the IM-based method provides satisfying accuracy in predicting the median of the fragility curves for this type of structures.

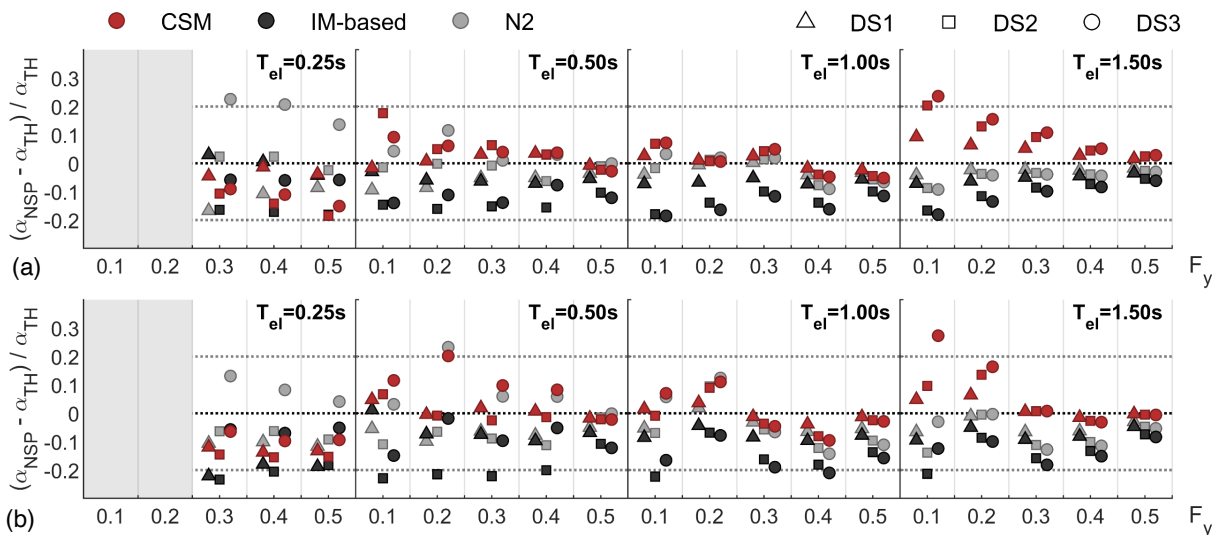
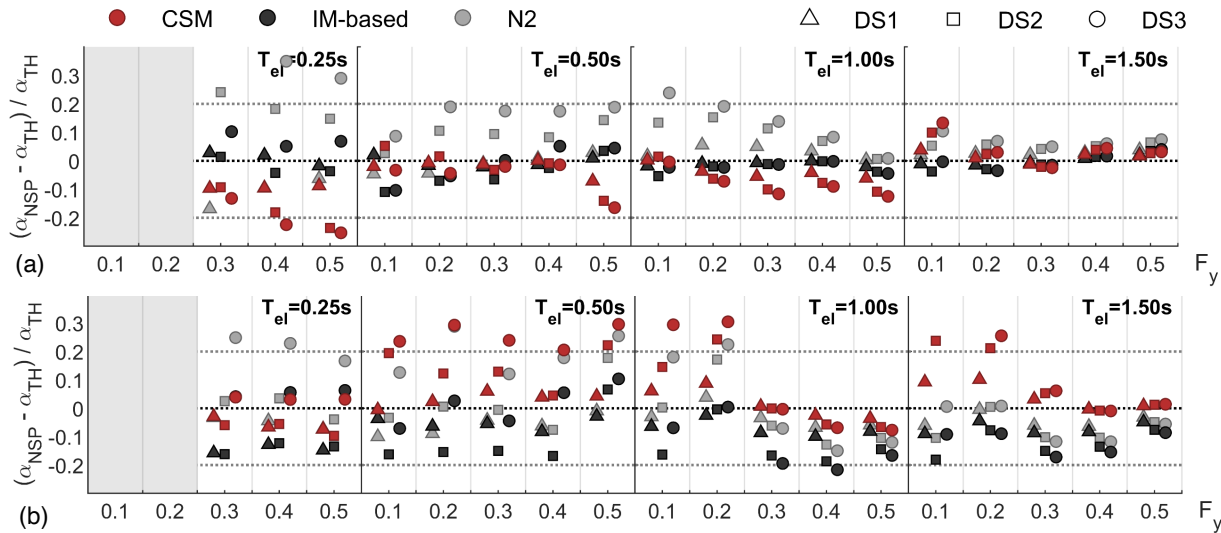


Figure 14. NSP-vs-NLTHA relative errors on the median IM( $\alpha$ ) for the SDoF systems with period equal to 0.25 s, 0.50 s, 1.00 s and 1.50 s and MTf (a) / BIL (b) hysteresis rule ( $\mu = 3$ ,  $F_r = 0.6F_y$ ,  $r = 0\%$ ).



**Figure 15.** NSP-vs-NLTHA relative errors on the median IM ( $\alpha$ ) for the SDoF systems with period equal to 0.25, 0.50, 1.00 and 1.50 s and FS (a) / EPP (b) hysteresis rule ( $\mu = 3, F_r = 0.6F_y, r = 0\%$ ).

On the other hand, lower values of the CSM target displacements are expected for EPP, observing the high value of  $C_{evd}$  (equal to 0.670). In this case, Figure 15b shows that for elastic periods equal to 0.50 s, the CSM systematically overestimates the NLTHA-based median since it provides lower performance displacements with respect to the NLTHA. This can be caused by a too-large value of the EPP-based equivalent viscous damping or by the high sensitivity to the record duration of the response of SDoF systems characterised by an EPP hysteretic behaviour. Further information about this latter phenomenon is reported in Priestley et al. [30], stating that long-duration ground motions could involve “crawling” displacement for EPP systems. As an example, the results of the oscillator with elastic period and base shear coefficient equal to 0.50 s and 0.2 respectively can be analysed. In this case,  $\alpha_{DS3}$  calculated via NLTHA is equal to 0.55 g and 0.64 g if EPP or MTF are respectively used. The higher fragility detected in the former case disagrees with the corresponding higher value of  $C_{evd}$  which is a proxy of larger dissipation and thus lower ductility demand with respect to the MTF hysteretic behaviour. This shows the loss of accuracy of the CSM in this case, which provides  $\alpha_{DS3}$  equal to 0.7 g and 0.67 g respectively.

For the sake of completeness, Figure 16 reports the values of the dispersion for DS3 calculated through the CSM and NLTHA for the MTF and FS subgroups adopting *AvgSa* as IM. The results of the N2 and IM-based methods are not shown in the figure, given the considerations reported in the previous sub-section. Consistently with the MTF, it is evident that the Cloud-CSM induces an overestimation in the dispersion, which is higher for a high inelastic response (for example, caused by a low base shear coefficient). Moreover, the CSM-vs-NLTHA differences in  $\beta_{DS3}$  increase in the cases where the accuracy of the CSM concerning  $\alpha_{DS3}$  decreases. This can be easily observed for the oscillators having an elastic period equal to 0.25 s for both MTF and FS subgroups.

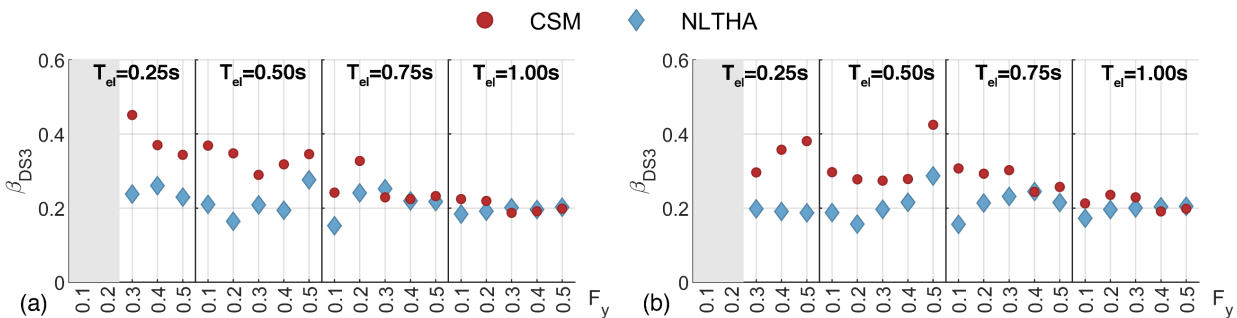


**Figure 16.** Dispersion ( $\beta$ ) at DS3 estimated by the CSM and NLTHA for the considered subgroup ( $\mu = 3, F_r = 0.6F_y, r = 0\%$ ) for MTF (a) and FS (b).

#### 5.4 Influence of other backbone parameters

640

The sensitivity of the effectiveness of the Cloud-CSM to the variation of significant backbone parameters is discussed in this sub-section. Particularly, Figure 17 shows the errors on the median of the fragility curves of the CSM with respect to the NLTHA for different values of the ductility at maximum strength, the residual base shear strength at collapse and the hardening ratio. Various subgroups of oscillators are considered for illustrative purpose, whose backbone parameters are listed in the legends of the figures. Figure 17a, b and c are aimed at discussing the influence of varying ductility capacity equal to 1.5 and 4.5. The results of the SDoF system having a period equal to 0.25 s are excluded for the same reason mentioned in Section 5.2. These outcomes demonstrate a low influence of the ductility capacity on the results of the Cloud-CSM within the Modified Takeda subgroups. Indeed, the maximum difference is detected for the SDoF with an elastic period equal to 1.50 s and MTf where the errors for the DS3 fragility median raise from 5% to 12%. In this case, the probabilistic seismic demand models related to low and high ductility are very similar since the backbones are practically identical until the reaching of the DS2, and only the 6% of the ground motions push the former case (low ductility) beyond this limit (i.e., the cloud data almost match). This means that the different errors are only linked to the propagation of the differences between the NLTHA- and CSM-based power-law models approaching the DS2 and DS3 thresholds, which in the high-ductility cases correspond to high inelastic response with respect to the low-ductility one. The sensitivity of the CSM to the variation of the parameter  $\mu$  is enhanced for the EPP rule (Figure 17c). In this case, if the ductility capacity is low, the softening branch is prematurely reached, and consequently, the inaccuracies discussed in the previous section are emphasized. Conversely, if the ductility capacity increases, the accuracy of the Cloud-CSM increases.

645

650

655

660

Figure 17d, e and f report the sensitivity of the CSM-vs-NLTHA relative errors on  $\alpha$  for oscillators with variable residual strength at collapse ( $F_r$  equal to  $0.6F_y$  and  $0.3F_y$ ). It is evident that the decreasing residual strength induces increasing error in the cases with a short-to-medium elastic period where a high number of ground motions pushes the SDoF to the softening and residual strength branches. The loss of accuracy of the CSM is caused by the  $C_{evd}$  coefficients which, being originally calibrated to support displacement-based design approaches, may be less reliable in considering the decreasing hysteretic dissipation in the softening and residual strength branches. For this reason, when a consistent number of ground motions requires a performance displacement higher than the displacement at DS2, the CSM underestimates the NLTHA-based target displacement, overestimating the median of the fragility curves. As an example, for MTf the errors at DS3 are 42% and 38% (out of bounds in the figure) for the oscillators with an elastic period equal to 0.75 and 1.00 s (Figure 17d). For the MTt subgroup similar results with respect to the MTf one are observed, but not shown for brevity.

665

670

675

Figure 17g, h, and i show the sensitivity of the accuracy of the CSM on varying values of hardening ratio ( $r$  equal to 0% and 10%) for MTt, MTf and FS subgroups. Note that an increasing hardening ratio induces a decreasing hysteretic dissipation which is not considered by the ductility-based equivalent viscous damping formulations. Accordingly, Figure 17g and h (MTf and MTt) indicate that, for hardening equal to 10%, the CSM increasingly overestimates the median estimated by NLTHA with respect to hardening equal to 0%. As an example, for the oscillator having an elastic period equal to 0.75 s and MTt, the error at DS3 increases from 9% to 21%.

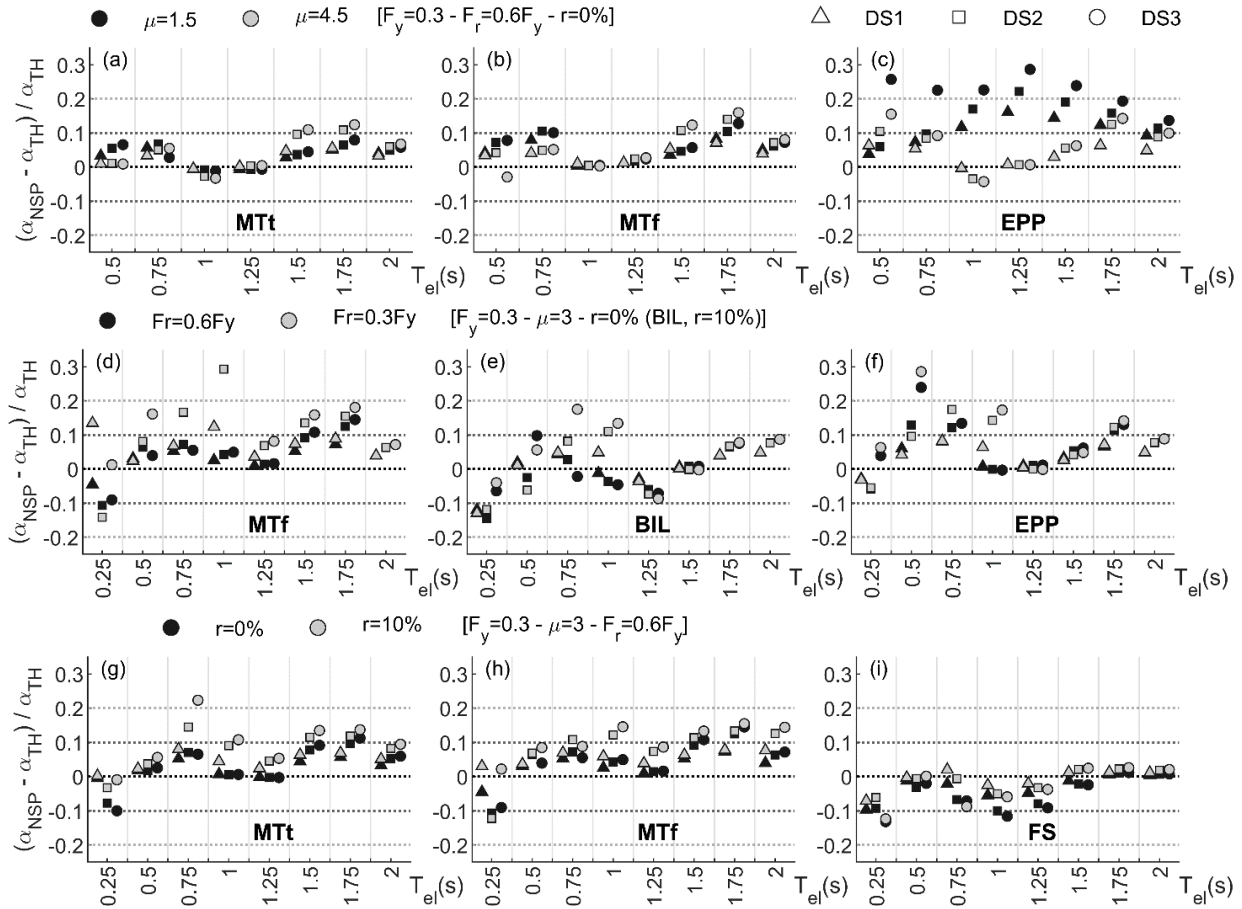


Figure 17. CSM-vs-NLTHA relative errors on the median IM ( $\alpha$ ) on varying ductility capacity (a-c), residual strength (d-f) and hardening ratio (g-i) for different hysteresis rules.

## 6. OVERVIEW OF THE CLOUD-CSM AND FINAL RECOMMENDATIONS

680

This section summarizes the steps of the Cloud-CSM with appropriate recommendations for users interested in applying the proposed method, according to the findings of Section 4 and 5. Figure 18 provides a flowchart of the Cloud-CSM indicating the different application modules. Recommendations to perform an initial record selection (Module 1) and the cloud approach for fragility analysis (Module 4) are provided in [33] and in Section 3.3. Further information about the proposed CSM algorithm using real ground-motion spectra (Module 2) is provided in Section 3.1. Note that other state-of-the-art equivalent viscous damping formulations can be adopted, allowing for future refining of the method and application for other types of structures. Moreover, other fragility analysis approaches (e.g. multi-stripe analysis) can be used (Module 4), provided that an appropriate initial record selection (and scaling) is performed.

690

Within the analysed values of elastic period and base shear coefficient ( $0.25 \text{ s} \leq T_{el} \leq 2.00 \text{ s}$ ;  $0.1 \leq F_y \leq 0.5$ ), the proposed Cloud-CSM approach shows promising accuracy in estimating seismic fragility, provided that reliable hysteresis-dependent equivalent viscous damping formulations are adopted (MTt, MTf, BIL and FS). Ductility capacity and hardening can slightly affect the accuracy of the proposed method. However, the authors recommend not using the proposed methodology for structures with a combination of high period and low strength ( $T_{el} \geq 1.50 \text{ s}$  &  $F_y \leq 0.2$ ). In this case, the adopted equivalent viscous damping formulations provide unsatisfactory results.

695

For these cases, the N2 method or the IM-based method proposed in Section 5.1 lead to higher accuracy in performance displacement prediction. Note that the accuracy of the Cloud-CSM can decrease for structures characterised by a large within-cycle strength degradation (i.e. low residual strength at collapse) for an increasing number of ground-motion responses in the softening branch. The estimates of the Cloud-CSM can be also biased for structures having an elastic-perfectly plastic backbone with kinematic hardening hysteresis behaviour (EPP subgroup), particularly for low values of ductility capacity.

700

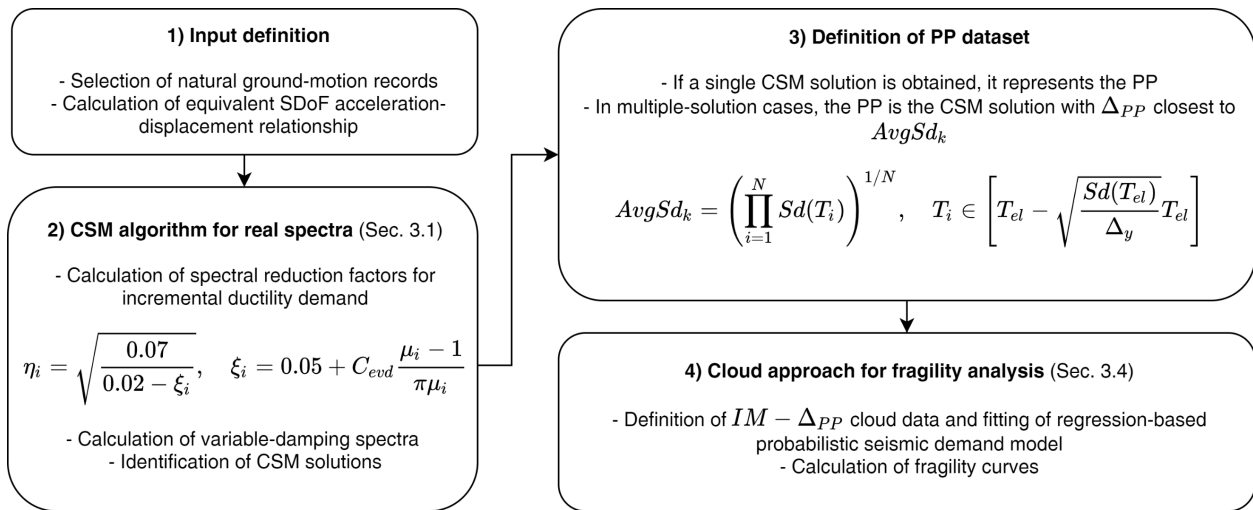


**Figure 18. Recommendations to apply the Cloud-CSM**

705 **7. CONCLUSIONS**

In this study, the Capacity Spectrum Method (CSM) effectiveness in performing seismic fragility analysis accounting for record-to-record variability is discussed with application to a case-study database of 2160 single-degree-of-freedom (SDoF) systems and 100 as-recorded, unscaled ground motions. Multi-linear parametric backbone curves represent SDoF systems with a different elastic period, yield base shear coefficient, ductility capacity, hardening ratio, residual strength. Five types of hysteresis are also adopted: Modified Takeda Fat, Modified Takeda Thin, Elastic-Perfectly Plastic, Bilinear and Flag-Shaped. An efficient algorithm to perform the CSM with real, as-recorded spectra is proposed, combined with a cloud-based approach (Cloud-CSM) to derive fragility relationships. Simple criteria to solve the issue of multiple CSM solutions (i.e., two or more points on the backbone satisfying the CSM procedure) are proposed and tested. The effectiveness of the Cloud-CSM in fragility analysis is discussed through comparisons with more refined nonlinear time history analyses (NLTHA), the N2 method and a simple method involving an intensity measure as a direct proxy for the performance displacement. The results of this study can be summarised as follows.

- The CSM applied with real spectra may produce multiple solutions which are not physics-based. The effectiveness of different criteria (based on simplistic assumption or efficient intensity measures) in selecting the performance point is analysed. It is demonstrated that an effective strategy involves selecting the CSM solution with a performance displacement closest to the geometric average of the spectral displacements calculated in an appropriate range of periods.
- The influence of multiple-solution cases in fragility analysis is studied. It is demonstrated that an incorrect choice of the performance point may imply errors on the median and dispersion of the fragility curves higher than 20%, if more than 20% of the adopted ground motions lead to multiple solutions. If an appropriate performance point selection is performed, the errors can be strongly reduced (lower than 5%) regardless of the number of multiple-solution cases.
- It is shown that in most of the analysed cases, the Cloud-CSM provides errors lower than  $\pm 20\%$  in predicting the median. The accuracy of this method decreases (errors higher than 20%) for: cases characterised by a combination of low strength and long period ( $T_{el} \geq 1.50s$  &  $F_y \leq 0.2$ ); cases showing very high within-cycle strength degradation; cases with an elastic-perfectly plastic backbone and kinematic hardening hysteretic model.
- In most of the analysed short- or medium-period cases, the CSM provides a higher or comparable accuracy with respect to the N2 method and the proposed simplistic intensity measure-based method, which predicts the performance displacement only based on spectral ordinates. The N2 can provide noticeable inaccuracies (errors higher than 20%) with reference to flag-shaped hysteresis or an elastic-perfectly plastic backbone and kinematic hardening hysteretic model.
- The N2 and the proposed intensity measure-based method for performance displacement identification can strongly underestimate the dispersion in fragility curves (resulting in low predicted seismic risk) depending

on the adopted intensity measure. Contrarily, the Cloud-CSM can be applied regardless of the selected intensity measure. This latter implies an increasing dispersion in the fragility relationships with respect to NLTHA.

745 Given the low computational effort required, the Cloud-CSM can accurately support applications where a large number of analyses is generally involved, such as regional-scale assessment of portfolios of structures or characterisation of epistemic uncertainties in archetype structures. Future studies aimed at developing more refined formulations of equivalent viscous damping coefficients, possibly dependent on the backbone and/or hysteresis parameters, could substantially improve the accuracy of the CSM in fragility analysis of existing structures. Also, further developments could contribute to test the accuracy of the CSM applied with real spectra, considering the effects of specific ground motion characteristics (e.g. pulse-like ground motions [47,48]).

750 For practical applications on MDoF structures, deemed to be the scope of Cloud-CSM, the bias due to the transformation of the refined MDoF pushover curve to the SDoF multi-linear one should be carefully checked on a case-by-case basis if no typology-specific literature studies that characterize this bias are available.

## 755 ACKNOWLEDGEMENTS

This study was part of the Industrial PhD research program (PON-RI 2014-2020) sponsored by the Italian Ministry of University and Research (DOT130UZWT). The second author received funding from the European Union's Horizon 2020 research and innovation program under grant agreement No. 843794 (Marie Skłodowska-Curie Research Grants Scheme MSCA-IF-2018: Multi-level Framework to Enhance Seismic Resilience of RC buildings (MULTIRES)).

## 760 REFERENCES

- 765 [1] Silva V, Crowley H, Varum H, Pinho R, Sousa R. Evaluation of analytical methodologies used to derive vulnerability functions. *Earthq Eng Struct Dyn* 2014. <https://doi.org/10.1002/eqe.2337>.
- [2] Silva V, Akkar S, Baker J, Bazzurro P, Castro JM, Crowley H, et al. Current challenges and future trends in analytical fragility and vulnerability modeling. *Earthq Spectra* 2019. <https://doi.org/10.1193/042418EQS1010>.
- 770 [3] Gentile R, Galasso C. Gaussian process regression for seismic fragility assessment of building portfolios. *Struct Saf* 2020. <https://doi.org/10.1016/j.strusafe.2020.101980>.
- [4] Sevieri G, Gentile R, Galasso C. A bayesian framework for robust seismic fragility assessment based on various model classes. 17th World Conf. Earthq. Eng., Sendai, Japan: 2020.
- [5] Fajfar P. Capacity spectrum method based on inelastic demand spectra. *Earthq Eng Struct Dyn* 1999;28:979–93. [https://doi.org/10.1002/\(SICI\)1096-9845\(199909\)28:9<979::AID-EQE850>3.0.CO;2-1](https://doi.org/10.1002/(SICI)1096-9845(199909)28:9<979::AID-EQE850>3.0.CO;2-1).
- 775 [6] Fajfar P, Gašperšič P. The N2 method for the seismic damage analysis of RC buildings. *Earthq Eng Struct Dyn* 1996. [https://doi.org/10.1002/\(SICI\)1096-9845\(199601\)25:1<31::AID-EQE534>3.0.CO;2-V](https://doi.org/10.1002/(SICI)1096-9845(199601)25:1<31::AID-EQE534>3.0.CO;2-V).
- [7] CEN. Eurocode 8 (EN 1998-3: 2004) Design of structures for earthquake resistance—Part 3: Assessment and retrofitting of buildings. Brussels, Belgium: 2005.
- [8] FEMA-273. NEHRP guidelines for the seismic rehabilitation of buildings. Washington DC, USA: 1997.
- 780 [9] Freeman SA. Development and use of capacity spectrum method. Proc 6th US NCEE Conf Earthq Eng 1998.
- [10] ATC. Applied Technology Council (ATC-40) - Seismic evaluation and retrofit of concrete buildings 1996.
- [11] FEMA. Improvement of Nonlinear Static Seismic Analysis Procedures. FEMA 440, Fed Emerg Manag Agency, Washingt DC 2005.
- 785 [12] Casarotti C, Pinho R. An adaptive capacity spectrum method for assessment of bridges subjected to earthquake action. *Bull Earthq Eng* 2007;5:377–90. <https://doi.org/10.1007/s10518-007-9031-8>.
- [13] Ruiz-García J, Miranda E. Inelastic displacement ratios for evaluation of existing structures. *Earthq Eng Struct Dyn* 2003;32:1237–58. <https://doi.org/10.1002/eqe.271>.
- [14] Lin Y-Y, Miranda E. Noniterative Equivalent Linear Method for Evaluation of Existing Structures. *J Struct Eng* 2008. [https://doi.org/10.1061/\(asce\)0733-9445\(2008\)134:11\(1685\)](https://doi.org/10.1061/(asce)0733-9445(2008)134:11(1685)).
- 790 [15] Lin YY, Chang KC. An improved capacity spectrum method for ATC-40. *Earthq Eng Struct Dyn* 2003. <https://doi.org/10.1002/eqe.312>.
- [16] Ruiz-García J, Miranda E. Probabilistic estimation of maximum inelastic displacement demands for performance-based design. *Earthq Eng Struct Dyn* 2007. <https://doi.org/10.1002/eqe.680>.
- 795 [17] Miranda E, Ruiz-García J. Evaluation of approximate methods to estimate maximum inelastic displacement demands. *Earthq Eng Struct Dyn* 2002. <https://doi.org/10.1002/eqe.143>.

- [18] Lin YY, Miranda E. Evaluation of equivalent linear methods for estimating target displacements of existing structures. *Eng Struct* 2009;31:3080–9. <https://doi.org/10.1016/j.engstruct.2009.08.009>.
- [19] Dolšek M. Simplified method for seismic risk assessment of buildings with consideration of aleatory and epistemic uncertainty. *Struct Infrastruct Eng* 2012;8:939–53. <https://doi.org/10.1080/15732479.2011.574813>.
- [20] Rossetto T, Gehl P, Minas S, Galasso C, Duffour P, Douglas J, et al. FRACAS: A capacity spectrum approach for seismic fragility assessment including record-to-record variability. *Eng Struct* 2016;125:337–48. <https://doi.org/10.1016/j.engstruct.2016.06.043>.
- [21] Vamvatsikos D, Cornell CA. Direct estimation of the seismic demand and capacity of oscillators with multi-linear static pushovers through IDA. *Earthq Eng Struct Dyn* 2006. <https://doi.org/10.1002/eqe.573>.
- [22] D'Ayala D, Meslem A, Vamvatsikos D, Porter K, Rossetto T, Crowley H, et al. Guidelines for Analytical Vulnerability Assessment - Low/Mid-Rise. *GEM Tech Rep* 2013;08:162. <https://doi.org/10.13117/GEM.VULN-MOD.TR2014.12>.
- [23] Gentile R, Galasso C, Pampanin S. Materials vs structural detailing : relative effect of their epistemic uncertainties on the seismic fragility of reinforced concrete frames. *J Struct Eng* 2020;in press. [https://doi.org/10.1061/\(ASCE\)ST.1943-541X.0002917](https://doi.org/10.1061/(ASCE)ST.1943-541X.0002917).
- [24] Giordano N, De Luca F, Sextos A. Analytical fragility curves for masonry school building portfolios in Nepal. *Bull Earthq Eng* 2021. <https://doi.org/10.1007/s10518-020-00989-8>.
- [25] Smerzini C, Galasso C, Iervolino I, Paolucci R. Ground motion record selection based on broadband spectral compatibility. *Earthq Spectra* 2014;30:1427–48. <https://doi.org/10.1193/052312EQS197M>.
- [26] Chopra A, Goel R. *Capacity-Demand-Diagram Methods for Estimating Seismic Deformation of Inelastic Structures: SDF Systems*. 1999.
- [27] Gentile R, Galasso C. Simplicity versus accuracy trade-off in estimating seismic fragility of existing reinforced concrete buildings. *Soil Dyn Earthq Eng* 2021. <https://doi.org/10.1016/j.soildyn.2021.106678>.
- [28] Şadan OB, Petrini L, Calvi GM. Direct displacement-based seismic assessment procedure for multi-span reinforced concrete bridges with single-column piers. *Earthq Eng Struct Dyn* 2013. <https://doi.org/10.1002/eqe.2257>.
- [29] Gentile R, Nettis A, Raffaele D. Effectiveness of the Displacement-Based seismic performance Assessment for continuous RC bridges and proposed extensions. *Eng Struct* 2020;in press:110910. <https://doi.org/10.1016/j.engstruct.2020.110910>.
- [30] Priestley MJN, Calvi GM, Kowalsky MJ. *Displacement-based seismic design of structures*. IUSS Press, Pavia, Italy; 2007.
- [31] Villar-Vega M, Silva V, Crowley H, Yepes C, Tarque N, Acevedo AB, et al. Development of a fragility model for the residential building stock in South America. *Earthq Spectra* 2017. <https://doi.org/10.1193/010716EQS005M>.
- [32] Martins L, Silva V. Development of a fragility and vulnerability model for global seismic risk analyses. *Bull Earthq Eng* 2020. <https://doi.org/10.1007/s10518-020-00885-1>.
- [33] Jalayer F, Ebrahimian H, Miano A, Manfredi G, Sezen H. Analytical fragility assessment using unscaled ground motion records. *Earthq Eng Struct Dyn* 2017;46:2639–63. <https://doi.org/10.1002/eqe.2922>.
- [34] Otani S. *SAKE: A COMPUTER PROGRAM FOR INELASTIC RESPONSE OF R/C FRAMES TO EARTHQUAKES*. Ill Univ Dep Civ Eng Struct Res Ser 1974.
- [35] Haselton CB, Baker JW, Liel AB, Deierlein GG. Accounting for Ground-Motion Spectral Shape Characteristics in Structural Collapse Assessment through an Adjustment for Epsilon. *J Struct Eng* 2011. [https://doi.org/10.1061/\(asce\)st.1943-541x.0000103](https://doi.org/10.1061/(asce)st.1943-541x.0000103).
- [36] Carr AJ. *RUAUMOKO3D - The Maori God of Volcanoes and Earthquakes*. Inelastic Analysis Finite Element program- Tech. Rep. 2016.
- [37] Lagomarsino S. Seismic assessment of rocking masonry structures. *Bull Earthq Eng* 2015. <https://doi.org/10.1007/s10518-014-9609-x>.
- [38] De Luca F, Vamvatsikos D, Iervolino I. Near-optimal piecewise linear fits of static pushover capacity curves for equivalent SDOF analysis. *Earthq Eng Struct Dyn* 2013. <https://doi.org/10.1002/eqe.2225>.
- [39] Ceballos C JL, Sullivan TJ. Development of improved inelastic displacement prediction equations for the seismic design of hybrid systems. *Bull New Zeal Soc Earthq Eng* 2012;45:1–14. <https://doi.org/10.5459/bnzsee.45.1.1-14>.
- [40] Khan E, Kowalsky MJ, Nau JM. Equivalent Viscous Damping Model for Short-Period Reinforced Concrete Bridges. *J Bridg Eng* 2016;21. [https://doi.org/10.1061/\(ASCE\)BE.1943-5592.0000803](https://doi.org/10.1061/(ASCE)BE.1943-5592.0000803).
- [41] Pennucci D, Sullivan TJ, Calvi GM. Displacement reduction factors for the design of medium and long

- period structures. *J Earthq Eng* 2011;15:1–29. <https://doi.org/10.1080/13632469.2011.562073>.
- [42] Minas S, Galasso C. Accounting for spectral shape in simplified fragility analysis of case-study reinforced concrete frames. *Soil Dyn Earthq Eng* 2019;119:91–103. <https://doi.org/10.1016/j.soildyn.2018.12.025>.
- [43] Vidic T, Fajfar P, Fischinger M. Consistent inelastic design spectra: Strength and displacement. *Earthq Eng Struct Dyn* 1994. <https://doi.org/10.1002/eqe.4290230504>.
- [44] Calvi GM, Rodrigues D, Silva V. Introducing new design spectra derived from Italian recorded ground motions 1972 to 2017. *Earthq Eng Struct Dyn* 2018;47:2644–60. <https://doi.org/10.1002/eqe.3102>.
- [45] Freddi F, Padgett JE, Dall'Asta A. Probabilistic seismic demand modeling of local level response parameters of an RC frame. *Bull Earthq Eng* 2017. <https://doi.org/10.1007/s10518-016-9948-x>.
- [46] Modica A, Stafford PJ. Vector fragility surfaces for reinforced concrete frames in Europe. *Bull Earthq Eng* 2014. <https://doi.org/10.1007/s10518-013-9571-z>.
- [47] Gentile R, Galasso C. Accounting for directivity-induced pulse-like ground motions in building portfolio loss assessment. *Bull Earthq Eng* 2020. <https://doi.org/10.1007/s10518-020-00950-9>.
- [48] Chang Z, De Luca F, Goda K. Near-fault acceleration pulses and non-acceleration pulses: Effects on the inelastic displacement ratio. *Earthq Eng Struct Dyn* 2019. <https://doi.org/10.1002/eqe.3184>.
- [49] Cordova PP, Deierlein GG, Mehanny SSF, Cornell CA. Development of a two-parameter seismic intensity measure and probabilistic assessment procedure. Second US- 13 Japan Work Performance-Based Earthq Eng Methodol Reinf Concr Build Struct 2001.
- [50] Kohrangi M, Bazzurro P, Vamvatsikos D. Vector and scalar IMs in structural response estimation, Part II: Building demand assessment. *Earthq Spectra* 2016;32:1525–43. <https://doi.org/10.1193/053115EQS081M>.
- [51] Katsanos EI, Sextos AG. Inelastic spectra to predict period elongation of structures under earthquake loading. *Earthq Eng Struct Dyn* 2015. <https://doi.org/10.1002/eqe.2554>.
- [52] Mehanny SSF. A broad-range power-law form scalar-based seismic intensity measure. *Eng Struct* 2009;31:1354–68. <https://doi.org/10.1016/j.engstruct.2009.02.003>.
- [53] Kazantzi AK, Vamvatsikos D. Intensity measure selection for vulnerability studies of building classes. *Earthq Eng Struct Dyn* 2015. <https://doi.org/10.1002/eqe.2603>.

880

## APPENDIX

### A. Optimal IMs to select the PP

885 An efficient IM is by definition a good proxy of damage potentials, being highly correlated to EDPs such as the ductility demand or target displacement. In this appendix, an optimal IM analysis is performed. In fact, efficient IM(s) are used to define criteria for selecting the PP in CSM cases with multiple solutions (Section 3.2). This preliminary analysis examines spectral shape-dependent IMs, which can be easily extracted by the response spectrum which the CSM is based on. It is performed with reference to the results of NLTHA.

890 The dataset of candidate IMs is composed of both conventional and advanced structure-specific IMs. First, the spectral displacement at the elastic period,  $Sd(T_{el})$  is selected as a candidate IM. The second candidate IM is the displacement demand at corner period ( $T_D$ ), calculated as 90% of the maximum displacement demand, as suggested by Calvi et al. [44]. This IM is herein indicated as  $Sd(T_D)$ . It is well-recognized in the literature that efficient spectral shape-based IMs allow accounting for the spectral demand in the period elongation range, particularly in the case of strong inelastic response. Consequently, the third IM is a displacement-based version of the IM proposed by Cordova [49] ( $Sd^c$ , Equation A1) which considers the contribution of the ratio of the spectral demands calculated at the elongated and at the elastic periods. The authors recommend a value of period elongation equal to  $2T_{el}$  ( $c = 2$ ). Recent studies [42,50] investigated the efficiency of IMs based on the geometric average of the spectral accelerations over an appropriate range of periods (usually named *AvgSa*). In this study, since the displacements are of interest, the geometric average of the spectral displacements is added in the IM dataset (Equation A2).

900

$$Sd^c = Sd(T_{el})\sqrt{Sd(cT_{el})/Sd(T_{el})} \quad (A1)$$



$$AvgSd(T_{el} - kT_{el}) = \left( \prod_{i=1}^N Sd(T_i) \right)^{\frac{1}{N}} \text{ with } T_i \in [T_{el}, kT_{el}] \rightarrow \begin{cases} AvgSd_{1.5}, & k = 1.5 \\ AvgSd_2, & k = 2 \\ AvgSd_k, & k = \sqrt{Sd(T_{el})/\Delta_y} \end{cases} \quad (A2)$$

905 The period range should be adequate to consider the period elongation ( $kT_{el}$ ) due to the inelastic response. In contrast, values of period lower than  $T_{el}$ , which are associated with higher modes, are not considered herein, since this study focuses on SDoF systems. Katsanos & Sextos [51] demonstrated that the period elongation of SDoF systems ranges from 120% to 250% and strongly depends on the ratio between the yielding displacement with respect to the elastic displacement demand at the first period. Therefore, two versions of  $AvgSd$  are considered, setting  $k$  equal to 1.5 and  
 910 2 (respectively indicated as  $AvgSd_{1.5}$ ,  $AvgSd_2$  hereafter). Finally, a more advanced version of  $AvgSd$  is proposed ( $AvgSd_k$ ), assuming that the range of significant periods affecting the inelastic response depends on a specific-record proxy of the likely ductility demand as proposed in [52]. Consistently with [42], ten equally spaced periods ( $N = 10$ ) are used to compute  $AvgSd$ .

915 The optimal IM analysis is performed, considering only the NLTHA results leading to an inelastic response. In case of an elastic response, no multiple solutions can be retrieved via the CSM, and a perfect and deterministic correlation is observed between the displacement demand and  $Sd(T_{el})$ . Considering the maximum displacement of the SDoF system estimated by NLTHA as the EDP of interest, a power-law model ( $EDP = aIM^b$ ) is fitted to the “cloud data” in the  $\log IM - \log EDP$  plane and the parameters  $a$  and  $b$  are estimated (see Section 3.3). As confirmed by Minas and Galasso [42], the higher is the efficiency of the IM, the lower is the standard deviation ( $\sigma$ ) of the  $edp_{gm} - im_{gm}$   
 920 pairs corresponding to the  $gm$ -th record with respect to the linear statistical model in the logarithmic space. This logarithmic standard deviation (or dispersion) is quantified via Equation 7 in Section 3.3, where  $N$  is the number of inelastic-response ground motions.

To analyse the results, all the SDoF systems are grouped by elastic period and hysteretic behaviour; the average value of  $\sigma$  is estimated for each subgroup. Figure A1 shows the results for the MTf and FS subgroups, representative of high  
 925 and low cyclic dissipation. Additionally, Figure A2 reports the regression models calculated for two selected MTf case-studies ( $T_{el} = 0.75$  s,  $\mu = 3$ ,  $F_y$  equal to 0.1 and 0.4, respectively) and by using three selected IM candidates. These SDoF systems are subjected to different “average” nonlinearity level: in the first case the inelastic  $edp_{gm}$  are homogeneously distributed between the DS1 and collapse thresholds, while in the second case, most of the  $edp_{gm}$  are included between the DS1 and DS2 thresholds. It is evident that  $Sd(T_d)$  is the least efficient IM being totally  
 930 independent of structure-specific dynamic features (Figure A1). For both the cases reported in Figure A2b and e,  $\sigma$  is higher than 0.36. Figure A1 shows that  $Sd(T_{el})$  is a particularly good proxy for high-period oscillators that exhibit a low nonlinear demand. As an example,  $\sigma$  decreases from 0.234 to 0.197 considering the cases in Figure A2a and d.  $AvgSd_{1.5}$  demonstrates its efficiency for low-period SDoF systems, where a strong inelasticity is usually required and the influence of the spectral shape in the period elongation range is significant. It is worth noting that  $AvgSd_{1.5}$   
 935 outperforms  $AvgSd_2$  proving that elongation of  $1.5T_{el}$  is likely a better choice than  $2T_{el}$  with reference to the average features of these case studies.  $Sd^c$  provides an intermediate efficiency, comparable to the results of  $AvgSd_2$ . The best predictor is  $AvgSd_k$  which exhibits the lowest average standard deviation for all the subgroups of case studies. This is because this advanced IM adapts the period range given a proxy of the inelastic demand. For instance,  $\sigma$  is approximately equal to 0.15 in Figure A2c and f, and thus is negligibly affected by the average nonlinear demand of  
 940 the ground-motion suite. Further analyses could be performed to appropriately calibrate the discretisation of the period range in which  $AvgSd$  is calculated [42,53] or the  $c$  parameter for  $Sd^c$ , possibly with reference to a narrower subgrouping of the case-study dataset (e.g., grouped using the base shear coefficient). However, this task is deemed not consistent with the purposes of this study. The comparison between MTf and FS reported in Figure A1a and b demonstrates that these results are weakly affected by the adopted hysteresis rule.

945

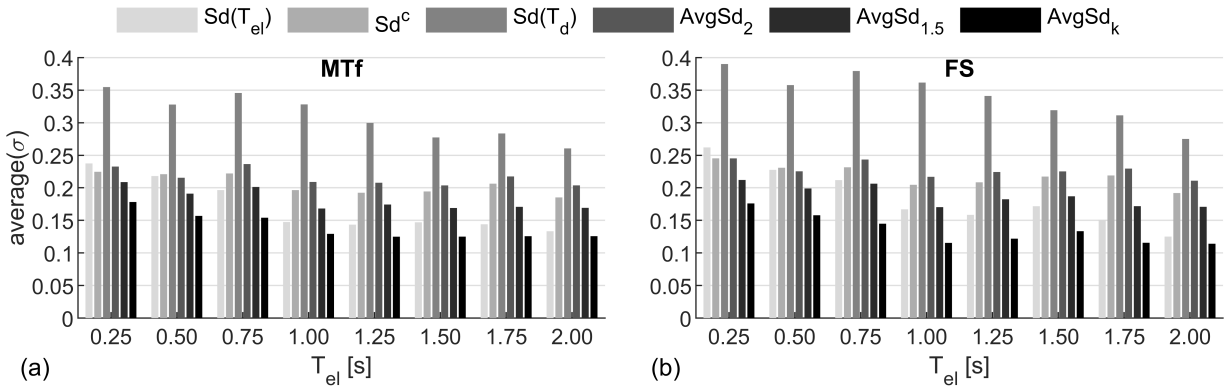


Figure A1. Average dispersion related to the candidate IMs for the MTf (a) and FS (b) subgroups.

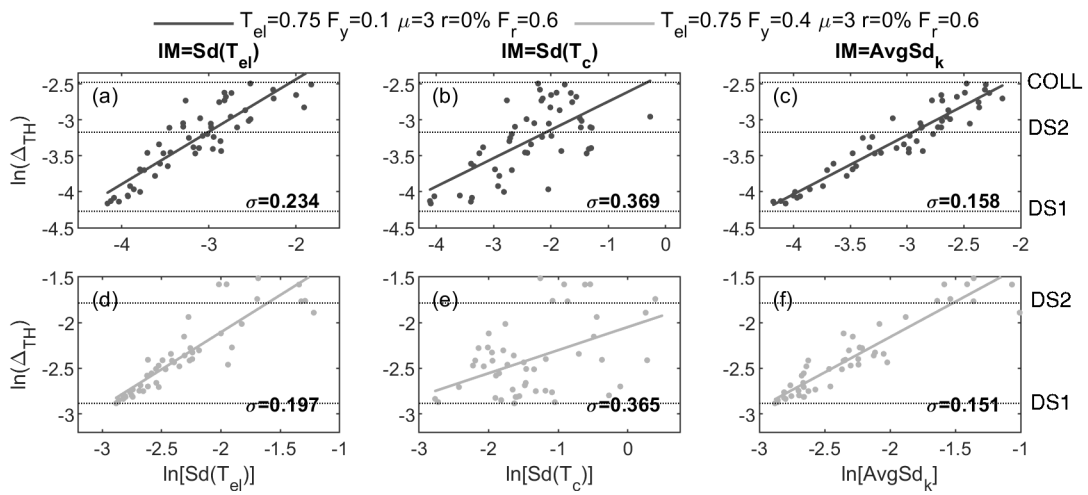


Figure A2. Regression analysis for two selected SDoF systems (MTf subgroup) varying the adopted IM.